

Efficient Parameter Estimation of Sampled Random Fields

Arthur P. Guillaumin¹, Adam M. Sykulski², Sofia C. Olhede^{3,1}
and Frederik J. Simons⁴

¹*University College London, UK*

²*Lancaster University, UK*

³*École polytechnique fédérale de Lausanne, Switserland*

⁴*Princeton University, USA*

Abstract

We provide a computationally and statistically efficient method for estimating the parameters of a stochastic Gaussian model observed on a spatial grid, which need not be rectangular. Standard methods are plagued by computational intractability, where designing methods that can be implemented for realistically sized problems has been an issue for a long time. This has motivated the use of the Fourier Transform and the Whittle likelihood approximation. The challenge of frequency-domain methods is to determine and account for observational boundary effects, missing data, and the shape of the observed spatial grid. In this paper we address these effects explicitly by proposing a new quasi-likelihood estimator. We prove consistency and asymptotic normality of our estimator, and show that the proposed method solves boundary issues with Whittle estimation for finite samples, yielding parameter estimates with significantly reduced bias and error. We demonstrate the effectiveness of our method for incomplete lattices, in comparison to other recent methods. Finally, we apply our method to estimate the parameters of a Matérn process used to model data from Venus' topography.

Keywords: Spatial Statistics, Quasi-likelihood, Computational efficiency, Statistical efficiency, Whittle likelihood

1 Introduction

Among the main challenges of modern data analysis is making sense of large volumes of spatial and spatiotemporal data. The application areas which require such methods are widespread including astrophysics and cosmology (e.g., Matsubara, 2004; Scargle et al., 2017), geophysical and planetary sciences (e.g., Aharonson et al., 2001; Goff and Arbic, 2010; Simons and Olhede, 2013), remote sensing (e.g., Candela et al., 2012; Maggiori et al., 2017), image and texture analysis (e.g., Eom, 2001; Jain et al., 2012), climate science (e.g., North et al., 2011; Sun et al., 2015), and environmetrics (e.g., Stein, 2007; Sáez et al., 2012). The variety and complexity of these examples show the utility of determining automated, fast, and exact, computational methods for spatial data analysis.

There are a number of challenges that must be resolved in the analysis of large volumes of spatial data including: i) removing estimation bias, ii) achieving computational tractability and iii) handling various shapes of data and missing observations. In this paper we propose novel methodology that simultaneously addresses all three challenges.

The state-of-the-art estimation methods currently in use are primarily reliant on spatial/pixel (Datta et al., 2016; Anitescu et al., 2017; Guinness and Fuentes, 2017; Katzfuss, 2017; Stroud et al., 2017) or spectral/wavenumber understanding (Kaufman et al., 2008; Shaby and Ruppert, 2012; Guinness, 2019). These recent advances have significantly enhanced our ability to perform inference on massive data sets. Our contribution is a methodology with further enhancements in terms of speed of implementation, coupled with a thorough theoretical understanding of the properties of finite but large samples.

It is widely recognized that in dimensions greater than one, boundary effects become problematic, especially in terms of bias (Dahlhaus and Künsch, 1987). To directly see the effects of this bias, observe Figure 1 where the top-left panel is an observation of topography from Venus (Rappaport et al., 1999). The bottom panels are realizations of a Matérn process, with parameters fitted to the data using the widely-used Whittle likelihood (see, e.g., Fuentes, 2007), with and without a taper. The simulated processes do not replicate the structure of the real data process, and this is due to boundary-effect bias as we show in this paper. The top-right panel uses parameters estimated from our methodology, which we call the *debiased* Whittle method. The resulting process is seen to more closely mimic the real data example, especially in terms of local smoothness, thus showing the importance of not just having access to a good model, but one with good parameter choices also.

The source of the bias which we remove is due to finite-domain effects, and to the boundary itself. Much of the literature on Whittle estimation has focused on modifications to the periodogram to reduce bias, such as tapering (Dahlhaus and Künsch, 1987), edge-effect estimation (Robinson and Sanz, 2006), or accounting for non-standard sampling scenarios (Fuentes, 2007; Matsuda and Yajima, 2009; Subba Rao, 2018). The solution we propose is simple yet effective: determine the true expectation of the periodogram, and construct a quasi-likelihood using this quantity rather than the true spectrum—further developing and generalizing a procedure recently proposed by Sykulski et al. (2019) for time series. We shall show that our debiased Whittle method almost completely removes estimation bias in spatial inference while leaving estimation variance essentially unaffected.

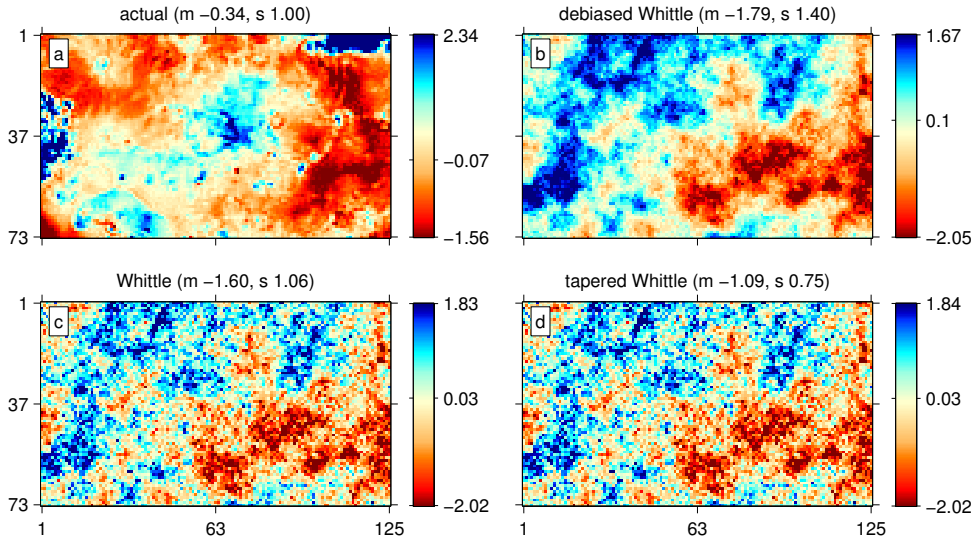


Figure 1: (a) A realized random field from the topography of Venus; and simulated random fields from a Matérn model with parameters estimated using (b) debiased Whittle estimation, (c) standard Whittle estimation, and (d) standard Whittle estimation using a Hanning taper. Parameter values for each method are given in Table 1 (Patch 3) in Section 5.3. Sample means (m) and standard deviations (s) are in the titles. Color bars are marked at the 2.5th, 50th and 97.5th quantiles. Axis labels are in pixels.

The notion of debiasing Whittle estimates using the expected periodogram has been previously proposed in Fernández-Casal and Crujeiras (2010), Simons and Olhede (2013), and Deb et al. (2017). This paper formalizes this estimation procedure by providing theoretical guarantees (via the concept of *significant correlation contribution*), as well as fast computational implementation, which apply to missing data, irregular grids, and any number of dimensions. Specifically, we will formally prove consistency and asymptotic normality of our estimator in a large-sample framework, and detail how the method is computed in $\mathcal{O}(|\mathbf{n}| \log |\mathbf{n}|)$ operations, where $|\mathbf{n}|$ is the number of observed data points.

This article provides the choice of notation and assumptions in Section 2. We propose our spatial quasi-likelihood in Section 3 and provide conditions guaranteeing consistent estimation under missing data. Section 4 develops our theoretical results. Section 5 shows the improved performance on simulated data, as well as an example of data analysis of the roughness of Venus’ topography. Finally we conclude with discussion in Section 6.

2 Notation and assumptions

Consider $X(\mathbf{s})$, for $\mathbf{s} \in \mathbb{R}^d$, where $d \geq 2$ is a positive integer. We denote the covariance function of $X(\mathbf{s})$ by $c_X(\mathbf{u})$, $\mathbf{u} \in \mathbb{R}^d$, and assume the existence of a positive piecewise

continuous spectral density function $f_X(\boldsymbol{\omega})$, such that $\forall \mathbf{u}, \mathbf{s} \in \mathbb{R}^d$,

$$c_X(\mathbf{u}) = \mathbb{E} \{X(\mathbf{s})X(\mathbf{s} + \mathbf{u})\} = \int_{\mathbb{R}^d} f_X(\boldsymbol{\omega}) \exp(i\boldsymbol{\omega} \cdot \mathbf{u}) d\boldsymbol{\omega}, \quad (1)$$

and $f_X(\boldsymbol{\omega}) = \int_{\mathbb{R}^d} c_X(\mathbf{u}) \exp(-i\boldsymbol{\omega} \cdot \mathbf{u}) d\mathbf{u}$. We shall assume the spectral density belongs to a parametric family indexed by the parameter $\boldsymbol{\theta} \in \Theta$, or $f_X(\boldsymbol{\omega}) = f(\boldsymbol{\omega}; \boldsymbol{\theta}_0)$, denoting the true parameter value by $\boldsymbol{\theta}_0 \in \Theta$. $X(\mathbf{s})$ is taken to be zero-mean, Gaussian, and homogeneous. We denote $\mathbf{n} = (n_1, \dots, n_d) \in (\mathbb{N}^+)^d$, with \mathbb{N}^+ the set of positive integers, the dimensions of an orthogonal rectangular grid, the *bounding grid*, defined by

$$\mathcal{J}_{\mathbf{n}} = \{\boldsymbol{\delta} \circ [x_1, \dots, x_d]^T : (x_1, \dots, x_d) \in \mathbb{N}^d, 0 \leq x_i \leq n_i - 1, i = 1, \dots, d\}, \quad (2)$$

and denote by $|\mathbf{n}| = \prod_{i=1}^d n_i$ the total number of points of this grid. We denote by $X_{\mathbf{s}}$, $\mathbf{s} \in \mathcal{J}_{\mathbf{n}}$ the values of the process on the grid. In (2), the quantity $\boldsymbol{\delta} \in (\mathbb{R}^+)^d$ indicates the regular spacing along each axis, with \mathbb{R}^+ the set of positive real numbers, and \circ denotes the pointwise, Hadamard product between two vectors. We always take $\boldsymbol{\delta} = [1, \dots, 1]^T$ for simplicity, unless stated otherwise. We write $f_{X,\boldsymbol{\delta}}(\boldsymbol{\omega})$ for the spectral density of the sampled process, the *aliased* spectral density, defined by

$$f_{X,\boldsymbol{\delta}}(\boldsymbol{\omega}) = \sum_{\mathbf{u} \in \mathbb{Z}^d} f_X(\boldsymbol{\omega} + 2\pi\mathbf{u}), \quad \boldsymbol{\omega} \in \mathbb{R}^d, \quad (3)$$

which is a Fourier pair with $c_X(\mathbf{u}) = \int_{\mathcal{T}^d} f_{X,\boldsymbol{\delta}}(\boldsymbol{\omega}) \exp(i\boldsymbol{\omega} \cdot \mathbf{u}) d\boldsymbol{\omega}$, $\forall \mathbf{u} \in \mathbb{Z}^d$, and $\mathcal{T} = [0, 2\pi)$, with \mathbb{Z} the set of natural integers.

To account for irregular shapes and missing data, we define a deterministic modulation value $g_{\mathbf{s}}$ at each location of the grid $\mathcal{J}_{\mathbf{n}}$. If a point on the grid is missing then $g_{\mathbf{s}} = 0$, otherwise $g_{\mathbf{s}} = 1$. By convention, $g_{\mathbf{s}}$ is extended to the whole set \mathbb{Z}^d , defining $g_{\mathbf{s}} = 0$ if $\mathbf{s} \notin \mathcal{J}_{\mathbf{n}}$. Using this notation, the periodogram of the observed data takes the form

$$I_{\mathbf{n}}(\boldsymbol{\omega}) = \frac{(2\pi)^{-d}}{\sum_{\mathbf{s} \in \mathcal{J}_{\mathbf{n}}} g_{\mathbf{s}}^2} \left| \sum_{\mathbf{s} \in \mathcal{J}_{\mathbf{n}}} g_{\mathbf{s}} X_{\mathbf{s}} \exp(-i\boldsymbol{\omega} \cdot \mathbf{s}) \right|^2, \quad \boldsymbol{\omega} \in \mathbb{R}^d, \quad (4)$$

where normalizing by $\sum_{\mathbf{s} \in \mathcal{J}_{\mathbf{n}}} g_{\mathbf{s}}^2$ rescales the periodogram for missing data, as performed in Fuentes (2007). Evaluating the periodogram at the set $\Omega_{\mathbf{n}} = \prod_{i=1}^d \{2\pi k n_i^{-1} : k = 0, \dots, n_i\}$ of Fourier frequencies corresponding to the grid $\mathcal{J}_{\mathbf{n}}$ requires $\mathcal{O}(|\mathbf{n}| \log |\mathbf{n}|)$ elementary operations using the Fast Fourier Transform (FFT). If a taper is used in the spectral estimate, then the values of the taper are directly incorporated into $g_{\mathbf{s}}$, such that $g_{\mathbf{s}}$ is proportional to the taper at locations where data is observed (and still set to zero otherwise).

3 Methodology

In Section 3.1 we introduce our new spatial frequency-domain quasi-likelihood estimator. In Section 3.2 we present an algorithm for the computation of the quasi-likelihood that

only requires FFTs, even in the scenario of missing data and general boundaries. Thus our estimation method uniquely retains the $\mathcal{O}(|\mathbf{n}| \log |\mathbf{n}|)$ computational cost of frequency-domain approaches for regular grids. Finally, in Section 3.3 we introduce the notion of *significant correlation contribution* for random fields, a set of sufficient conditions that ensures that our estimate is consistent under growing-domain asymptotics, despite the possibly non-regular shape of the data.

3.1 Estimation procedure

While exact likelihood has optimal statistical properties in the framework of an increasing domain (Mardia and Marshall, 1984), it is computationally inadequate for large data sets due to the determinant calculation and linear system that needs to be solved. A common approach is to trade off computational cost with statistical efficiency by using approximations of the likelihood function (Fuentes, 2007; Varin et al., 2011; Guinness and Fuentes, 2017). Such functions are commonly called quasi-likelihood methods. Our proposed estimation method is based on the following quasi-likelihood,

$$\ell_M(\boldsymbol{\theta}) = |\mathbf{n}|^{-1} \sum_{\boldsymbol{\omega} \in \Omega_{\mathbf{n}}} \left\{ \log \bar{I}_{\mathbf{n}}(\boldsymbol{\omega}; \boldsymbol{\theta}) + \frac{I_{\mathbf{n}}(\boldsymbol{\omega})}{\bar{I}_{\mathbf{n}}(\boldsymbol{\omega}; \boldsymbol{\theta})} \right\}, \quad (5)$$

where for all $\boldsymbol{\theta} \in \Theta$,

$$\bar{I}_{\mathbf{n}}(\boldsymbol{\omega}; \boldsymbol{\theta}) = \mathbb{E}_{\boldsymbol{\theta}}\{I_{\mathbf{n}}(\boldsymbol{\omega})\}, \quad (6)$$

that is to say, the expected periodogram on the grid $\mathcal{J}_{\mathbf{n}}$ given the modulation values $g_{\mathbf{s}}$, under the mean-zero Gaussian distribution specified by the parameter vector $\boldsymbol{\theta}$. Replacing $\bar{I}_{\mathbf{n}}(\boldsymbol{\omega}; \boldsymbol{\theta})$ with $f_X(\boldsymbol{\omega})$ in (5) yields the discretized form of the standard Whittle likelihood. Note however that unlike the spectral density, the expected periodogram depends on the dimensions of the lattice \mathbf{n} as well as the modulation values $g_{\mathbf{s}}$ accounting for missing points. We minimize (5) over Θ to obtain our estimate,

$$\hat{\boldsymbol{\theta}} = \arg \min_{\boldsymbol{\theta} \in \Theta} \{\ell_M(\boldsymbol{\theta})\}. \quad (7)$$

By minimizing (5), we find the maximum-likelihood estimate of the data under the following parametric model,

$$I_{\mathbf{n}}(\boldsymbol{\omega}) \stackrel{i.i.d.}{\sim} \text{Exp} \{ \bar{I}_{\mathbf{n}}(\boldsymbol{\omega}; \boldsymbol{\theta})^{-1} \}, \quad \boldsymbol{\omega} \in \Omega_{\mathbf{n}}, \quad (8)$$

where $\text{Exp}(\lambda)$ stands for the exponential distribution with parameter λ . Hence the quantity given in (5) can be seen as a composite likelihood (Varin et al., 2011; Bevilacqua and Gaetan, 2015). We also observe that $\Delta_{\boldsymbol{\theta}} \ell_M(\boldsymbol{\theta}_0) = \mathbf{0}$ such that our method fits within the general theory of estimating equations (Heyde, 1997; Jesus and Chandler, 2017).

3.2 Computation of the expected periodogram

In this section we show how the expected periodogram in (5) can be computed using FFTs such that our quasi-likelihood remains an $\mathcal{O}(|\mathbf{n}| \log |\mathbf{n}|)$ procedure. Direct calculations show that the expected periodogram is the convolution of the spectral density of the process with the multi-dimensional kernel $\mathcal{F}_{\mathbf{n}}(\boldsymbol{\omega})$,

$$\begin{aligned} \bar{I}_{\mathbf{n}}(\boldsymbol{\omega}; \boldsymbol{\theta}) &= \frac{(2\pi)^{-d}}{\sum_{\mathbf{s} \in \mathcal{J}_{\mathbf{n}}} g_{\mathbf{s}}^2} \{f_X(\cdot; \boldsymbol{\theta}) * \mathcal{F}_{\mathbf{n}}(\cdot)\}(\boldsymbol{\omega}) = \frac{(2\pi)^{-d}}{\sum_{\mathbf{s} \in \mathcal{J}_{\mathbf{n}}} g_{\mathbf{s}}^2} \int_{\mathbb{R}^d} f_X(\boldsymbol{\omega} - \boldsymbol{\omega}'; \boldsymbol{\theta}) \mathcal{F}_{\mathbf{n}}(\boldsymbol{\omega}') d\boldsymbol{\omega}' \\ &= \frac{(2\pi)^{-d}}{\sum_{\mathbf{s} \in \mathcal{J}_{\mathbf{n}}} g_{\mathbf{s}}^2} \int_{\mathcal{T}^d} f_{X,\delta}(\boldsymbol{\omega} - \boldsymbol{\omega}'; \boldsymbol{\theta}) \mathcal{F}_{\mathbf{n}}(\boldsymbol{\omega}') d\boldsymbol{\omega}', \end{aligned} \quad (9)$$

where

$$\mathcal{F}_{\mathbf{n}}(\boldsymbol{\omega}) = |\mathbf{n}|^{-1} \left| \sum_{\mathbf{s} \in \mathcal{J}_{\mathbf{n}}} g_{\mathbf{s}} \exp(i\boldsymbol{\omega} \cdot \mathbf{s}) \right|^2, \quad \boldsymbol{\omega} \in \mathbb{R}^d. \quad (10)$$

When $g_{\mathbf{s}} = 1 \forall \mathbf{s} \in \mathcal{J}_{\mathbf{n}}$, $\mathcal{F}_{\mathbf{n}}(\boldsymbol{\omega})$ is simply the multi-dimensional rectangular Féjer kernel. We now provide a lemma stating that the expected periodogram can be computed via two FFTs for any value of the modulation $g_{\mathbf{s}}$ on the grid $\mathcal{J}_{\mathbf{n}}$.

Lemma 1 (Computational efficiency of the expected periodogram). *The expected periodogram can be computed according to*

$$\bar{I}_{\mathbf{n}}(\boldsymbol{\omega}; \boldsymbol{\theta}) = (2\pi)^{-d} \sum_{\mathbf{u} \in \mathbb{Z}^d} \bar{c}_{\mathbf{n}}(\mathbf{u}; \boldsymbol{\theta}) \exp(-i\boldsymbol{\omega} \cdot \mathbf{u}), \quad (11)$$

where $\bar{c}_{\mathbf{n}}(\mathbf{u}; \boldsymbol{\theta})$ is defined by

$$\bar{c}_{\mathbf{n}}(\mathbf{u}; \boldsymbol{\theta}) = \frac{c_{g,\mathbf{n}}(\mathbf{u})}{c_{g,\mathbf{n}}(\mathbf{0})} c_X(\mathbf{u}; \boldsymbol{\theta}), \quad \mathbf{u} \in \mathbb{Z}^d, \quad (12)$$

$$c_{g,\mathbf{n}}(\mathbf{u}) = |\mathbf{n}|^{-1} \sum_{\mathbf{s} \in \mathcal{J}_{\mathbf{n}}} g_{\mathbf{s}} g_{\mathbf{s}+\mathbf{u}}, \quad \mathbf{u} \in \mathbb{Z}^d. \quad (13)$$

Proof. This is obtained by direct calculation on taking the expectation of the periodogram as defined in (4). \square

We remind the reader that $g_{\mathbf{s}}$ is defined to be zero outside $\mathcal{J}_{\mathbf{n}}$, such that $c_{g,\mathbf{n}}(\mathbf{u})$ is the ratio of the number of pairs of observations *separated* by the vector \mathbf{u} over the total number of points of the rectangular grid $\mathcal{J}_{\mathbf{n}}$. In the special case of complete observations on the rectangular grid (13) simplifies to

$$c_{g,\mathbf{n}}(\mathbf{u}) = \begin{cases} |\mathbf{n}|^{-1} \prod_{i=1}^d (n_i - |u_i|) & \text{if } |u_i| \leq n_i - 1, i = 1, \dots, d, \\ 0 & \text{otherwise.} \end{cases} \quad (14)$$

With missing values, $c_{g,\mathbf{n}}(\mathbf{u})$ can be precomputed for all relevant values of \mathbf{u} via an FFT independently of the parameter value $\boldsymbol{\theta}$, such that our method can be applied to scenarios of missing data without loss of computational efficiency. Similarly, we can combine our debiasing procedure with tapering by using a tapered spectral estimate for $I_{\mathbf{n}}(\boldsymbol{\omega})$ in (5) with adjusted values for $g_{\mathbf{s}}$ (as discussed at the end of Section 2). The expected periodogram, $\bar{I}_{\mathbf{n}}(\boldsymbol{\omega}; \boldsymbol{\theta})$, is then computed by using these values of $g_{\mathbf{s}}$ in the formulation of $c_{g,\mathbf{n}}(\mathbf{u})$ in (13). Combining debiasing and tapering therefore remains an $\mathcal{O}(|\mathbf{n}| \log |\mathbf{n}|)$ procedure.

3.3 Significant Correlation Contribution

To account for missing observations on the rectangular grid $\mathcal{J}_{\mathbf{n}}$, we replace missing values with zeros via the modulation function $g_{\mathbf{s}}$. Depending on $g_{\mathbf{s}}$ this may result in losing identifiability of the parameter vector from the second-order moment quantities available from the data. To avoid these issues we extend the notion of significant correlation, introduced by Guillaumin et al. (2017) for modulated time series, to the study of spatial data.

Definition 1 (Significant Correlation Contribution (SCC)). *A sequence of observed grids $(\mathcal{J}_{\mathbf{n}_k}, g_k)_{k \in \mathbb{N}}$ leads to significant correlation for the model family $\{f(\cdot; \boldsymbol{\theta}) : \boldsymbol{\theta} \in \Theta\}$ if,*

$$\liminf_{k \rightarrow \infty} S_k(\boldsymbol{\theta}_1, \boldsymbol{\theta}_2) > 0, \quad \forall \boldsymbol{\theta}_1 \neq \boldsymbol{\theta}_2 \in \Theta, \quad (15)$$

where $\liminf_{k \rightarrow \infty}$ denotes the limit inferior and where we have defined,

$$S_k(\boldsymbol{\theta}_1, \boldsymbol{\theta}_2) \equiv \sum_{\mathbf{u} \in \mathbb{Z}^d} \left\{ \frac{c_{g,\mathbf{n}_k}(\mathbf{u})}{c_{g,\mathbf{n}_k}(\mathbf{0})} \right\}^2 \{c_X(\mathbf{u}; \boldsymbol{\theta}_1) - c_X(\mathbf{u}; \boldsymbol{\theta}_2)\}^2. \quad (16)$$

The sum in (16) is *de facto* finite, due to the definition of $c_{g,\mathbf{n}}(\mathbf{u})$. Note that $c_{g,\mathbf{n}_k}(\mathbf{0})|\mathbf{n}_k|$ is the total number of observed points when no tapering is used. We observe that the above definition depends on both the sequence of grids, from $c_{g,\mathbf{n}_k}(\mathbf{u})$, and on the model family, from $c_X(\mathbf{u})$. In the rest of this paper we shall say that a sequence of grids leads to SCC, if the model family to which this applies is obvious from the context. SCC ensures that the expected periodograms for any two parameter vectors of the parameter set remain *asymptotically distant* (Bandyopadhyay and Lahiri, 2009). In Lemma 6 in Section 4, we show how this transfers to our approximate likelihood function. Then in Lemma 9 we show that the likelihood function converges uniformly in probability to its expectation over the parameter set, as long as $c_{g,\mathbf{n}_k}(\mathbf{0})|\mathbf{n}_k|$ goes to infinity. This all together will eventually lead to the consistency of our inference procedure, which is the result of Theorem 1.

Definition 1 extends the definition of SCC provided in Guillaumin et al. (2017) in two ways. First, it provides a generalization for spatial data. Secondly, even in one dimension, the version provided in Guillaumin et al. (2017) implies the version provided here, while the reverse is not always true—thus relaxing the assumptions required for consistency. We now provide more intuition of SCC via two lemmata.

Lemma 2 (SCC for fully observed rectangular grids). *In the scenario of a sequence of fully observed rectangular grids that grow unbounded in all directions (i.e., $n_i \rightarrow \infty$, $i = 1, \dots, d$, where we do not require that the growth happens with the same rate in all directions), SCC is equivalent to the standard assumption that for any two distinct parameter vectors $\boldsymbol{\theta}_1, \boldsymbol{\theta}_2 \in \Theta$, the measure of the set $\{\boldsymbol{\omega} \in \mathcal{T}^d : f_{X,\delta}(\boldsymbol{\omega}; \boldsymbol{\theta}_1) \neq f_{X,\delta}(\boldsymbol{\omega}; \boldsymbol{\theta}_2)\}$ is positive.*

Proof. Please see the Appendix. □

Note that we have required that the sequence of grids grows unbounded in all directions to obtain this equivalence when we have no further knowledge on the functional form of the spectral densities. However, in many practical cases, such as that of an exponential covariance function (see Appendix), we do not necessarily require this, which is an advantage of our method in comparison to standard frequency-domain methods.

Lemma 3 (Fixed shape of observations). *Consider a fixed shape defined by a function $\Xi : [0, 1]^d \mapsto \{0, 1\}$, and let $g_{k,\mathbf{s}} = \Xi(\mathbf{s} \circ \mathbf{n}_k^{-1}), \forall \mathbf{s} \in \mathcal{J}_{\mathbf{n}_k}, \forall k \in \mathbb{N}$. If the grids grow unbounded in all directions, and if the interior of the support of Ξ is not empty, then SCC is again equivalent to the condition stated in Lemma 2 on the parametric family of spectral densities.*

Proof. Please see the Appendix. □

Most importantly, one should note that SCC requires more than the fact that for two distinct parameters, the expected periodograms for the sequence of grids should never be equivalent, and this is to correctly account for missing data mechanisms and their impact on consistency.

4 Theory

In this section, we provide the proof of our estimator's consistency, derive its rate of convergence and its asymptotic distribution. We assume the following set of assumptions holds in order to establish consistency.

Assumption 1 (Consistency assumptions).

1. *The parameter set Θ is compact.*
2. *The aliased spectral density $f_{X,\delta}(\boldsymbol{\omega}; \boldsymbol{\theta}), \boldsymbol{\omega} \in \mathcal{T}^d, \boldsymbol{\theta} \in \Theta$ is bounded above by $f_{\delta,\max} < \infty$ and below by $f_{\delta,\min} > 0$. Additionally, $f_{X,\delta}(\boldsymbol{\omega}; \boldsymbol{\theta})$ admits a derivative with respect to the parameter vector $\boldsymbol{\theta}$, which is upper-bounded by $M_{\partial\theta}$.*
3. *The sequence of observation grids leads to SCC.*
4. *The number of actual observations $c_{g,\mathbf{n}_k}(\mathbf{0})|\mathbf{n}_k|$ grows to infinity as k goes to infinity.*
5. *The modulation $g_{\mathbf{s}}, \mathbf{s} \in \mathbb{Z}^2$, is upper bounded by a constant g_{\max} .*

Two main asymptotic frameworks coexist in spatial data analysis, infill asymptotics and growing-domain asymptotics (Zhang and Zimmerman, 2005). We study our estimator within the latter framework, which we consider most plausible for finite-resolution remote-sensing observations, imposing that $c_{g, \mathbf{n}_k}(\mathbf{0})|\mathbf{n}_k|$ goes to infinity while having fixed δ .

Theorem 1 (Consistency). *Under the set of Assumptions 1, the sequence of estimates $\hat{\boldsymbol{\theta}}_k$ defined by (7) converges in probability to the true parameter vector $\boldsymbol{\theta}$ as the observational domain diverges.*

This result holds for a wide class of practical applications, as we have *not* required:

- the rectangular grid to be fully observed. We allow for a wide class of observational domains, as long as the SCC is satisfied.
- the grid to grow at the same rate along all dimensions. Classical frequency-domain results make use of the fact that the multilevel Block Toeplitz with Toeplitz Blocks covariance matrix has its eigenvalues distributed as the spectral density. However this result only holds under the assumption that the sampling grid grows at the same rate along all dimensions.

We shall prove Theorem 1 in a series of steps, but start by introducing some new notation.

4.1 Additional notation

The vector of the values taken by the process on the rectangular grid $\mathcal{J}_{\mathbf{n}}$ is denoted $\mathbf{X} = [X_0, \dots, X_{|\mathbf{n}|-1}]^T$, where points are ordered into a vector according to the colexicographical order. Therefore in dimension $d = 2$, X_0, \dots, X_{n_1-1} are values from the first row of $\mathcal{J}_{\mathbf{n}}$, $X_{n_1}, \dots, X_{2n_1-1}$ are values from the second row, and so on. Similarly we denote \mathbf{g} the vector of the values taken by the modulation function on $\mathcal{J}_{\mathbf{n}}$, with points ordered in the same way. We also denote by $\mathbf{s}_0, \dots, \mathbf{s}_{|\mathbf{n}|-1}$ the locations of the grid ordered according to the same order, such that $X_0 = X(\mathbf{s}_0), X_1 = X(\mathbf{s}_1)$, etc.

We also denote by G the diagonal matrix with elements taken from \mathbf{g} , such that the vector corresponding to the observed random field (rather than \mathbf{X} which corresponds to the random field on the rectangular grid $\mathcal{J}_{\mathbf{n}}$) is given by the matrix product $G\mathbf{X}$.

Finally, for any vector \mathbf{V} we shall denote by $\|\mathbf{V}\|_p$ its \mathcal{L}_p norm (in particular $\|\cdot\|_2$ is the Euclidean norm), and for any $p \times p$ matrix A , $\|A\|$ shall denote the spectral norm, i.e., the \mathcal{L}_2 -induced norm,

$$\|A\| = \max_{\mathbf{v} \in \mathbb{R}^p, \mathbf{v} \neq \mathbf{0}} \frac{\|A\mathbf{v}\|_2}{\|\mathbf{v}\|_2}. \quad (17)$$

We remind the reader that if H is a Hermitian matrix, since $\|H\mathbf{V}\|_2^2 = \mathbf{V}^* H^* H \mathbf{V} = \mathbf{V}^* H^2 \mathbf{V}$, the spectral norm of H is its spectral radius, i.e.,

$$\|H\| = \rho(h) = \max\{|\lambda| : \lambda \text{ eigenvalue of } H\}. \quad (18)$$

4.2 Distributional properties of the periodogram

It is well known that the bias of the periodogram as an estimator of the spectral density is asymptotically zero (see, e.g., Koopmans, 1995). For finite samples however, the bias caused by leakage can be significant. Additionally, one can only estimate the aliased spectrum from a discretized sample of a continuous space process, which can lead to additional bias in the context of parametric estimation. As our method directly fits the expected periodogram rather than the spectral density, we need not be concerned by these issues, but the issue that remains is the correlation properties of the periodogram. We show that the variance of a bounded linear combination of the periodogram at Fourier frequencies goes to zero at a rate $\mathcal{O}\{(c_{g,\mathbf{n}}(\mathbf{0})|\mathbf{n}|)^{-1}\}$. This is the result of Proposition 1, which we use later in Lemma 9 to prove that our likelihood function converges uniformly in probability to its expectation.

Proposition 1 (Variance of linear functionals of the periodogram). *Let $a_{\mathbf{n}}(\boldsymbol{\omega})$ be a family of functions with support \mathcal{T}^d , indexed by $\mathbf{n} \in \mathbb{N}^d$ and uniformly bounded in absolute value. Then,*

$$\text{var} \left\{ |\mathbf{n}|^{-1} \sum_{\boldsymbol{\omega} \in \Omega_{\mathbf{n}}} a_{\mathbf{n}}(\boldsymbol{\omega}) I_{\mathbf{n}}(\boldsymbol{\omega}) \right\} = \mathcal{O} \{ (c_{g,\mathbf{n}}(\mathbf{0})|\mathbf{n}|)^{-1} \}. \quad (19)$$

Proof. Please see the Appendix. □

We observe that if $c_{g,\mathbf{n}}(\mathbf{0})$ goes to zero, i.e., if the ratio of the number of observed points to the total size of the grid goes to zero, then the variance of $|\mathbf{n}|^{-1} \sum_{\boldsymbol{\omega} \in \Omega_{\mathbf{n}}} a_{\mathbf{n}}(\boldsymbol{\omega}) I_{\mathbf{n}}(\boldsymbol{\omega})$ is altered. In the extreme case where $c_{g,\mathbf{n}}(\mathbf{0}) = \mathcal{O}(|\mathbf{n}|^{-1})$, the variance of the term under study behaves like a constant. This comes as no surprise since in that case the number of observed points is $\mathcal{O}(1)$.

4.3 Lemmata required for Theorem 1

We provide all the proofs of this section in the Appendix. To establish consistency we introduce some specific notation for the expectation of our quasi-likelihood,

$$\tilde{l}_{\mathbf{n}}(\boldsymbol{\gamma}) = \mathbb{E}_{\boldsymbol{\theta}} \{l_{\mathbf{n}}(\boldsymbol{\gamma})\} = |\mathbf{n}_k|^{-1} \sum_{\boldsymbol{\omega} \in \Omega_{\mathbf{n}_k}} \left\{ \log \bar{I}_{\mathbf{n}_k}(\boldsymbol{\omega}; \boldsymbol{\gamma}) + \frac{\bar{I}_{\mathbf{n}_k}(\boldsymbol{\omega}; \boldsymbol{\theta})}{\bar{I}_{\mathbf{n}_k}(\boldsymbol{\omega}; \boldsymbol{\gamma})} \right\}, \quad \forall \mathbf{n} \in (\mathbb{N}^+)^2, \forall \boldsymbol{\gamma} \in \Theta, \quad (20)$$

which we shall regard as a function of $\boldsymbol{\gamma}$. The following lemma states that this function attains its minimum at the true parameter vector (with no uniqueness property as of now).

Lemma 4 (Minimum of the expected quasi-likelihood function). *We have*

$$\tilde{l}_{\mathbf{n}}(\boldsymbol{\theta}) = \min_{\boldsymbol{\gamma} \in \Theta} \tilde{l}_{\mathbf{n}}(\boldsymbol{\gamma}; \boldsymbol{\theta}). \quad (21)$$

We shall also make repeated use of the following lemma.

Lemma 5 (Lower and upper bounds on the expected periodogram). *The expected periodogram satisfies, for all parameter vector $\gamma \in \Theta$, and at all wave-numbers $\omega \in \mathcal{T}^d$, for any $\mathbf{n} \in \mathbb{N}^d$,*

$$f_{\delta, \min} \leq \bar{I}_{\mathbf{n}_k}(\omega; \gamma) \leq f_{\delta, \max}.$$

We now provide two additional lemmata which are key to proving the consistency of our maximum quasi-likelihood estimator. Lemma 6 states that the expected likelihood value at a parameter vector distinct from the true parameter value is asymptotically bounded away from the expected likelihood at the true parameter value.

Lemma 6 (Identifiability from the expected likelihood function). *Let $\gamma \in \Theta$ distinct from θ . Then,*

$$\underline{\lim}_{k \rightarrow \infty} \left| \tilde{l}_{\mathbf{n}_k}(\gamma) - \tilde{l}_{\mathbf{n}_k}(\theta) \right| > 0, \quad (22)$$

where $\underline{\lim}_{k \rightarrow \infty}$ denotes the limit inferior as k goes to infinity.

Lemma 7 now states a form of continuity of our expected likelihood functions.

Lemma 7 (Continuity of the likelihood function). *Let $\gamma \in \Theta$ and let $(\gamma_k)_{k \in \mathbb{N}}$ be a sequence of parameter vectors that converges to γ . Then,*

$$\tilde{l}_{\mathbf{n}_k}(\gamma_k) - \tilde{l}_{\mathbf{n}_k}(\gamma) \longrightarrow 0, \quad (k \longrightarrow \infty). \quad (23)$$

Lemma 8. *Let $\gamma_k \in \Theta^{\mathbb{N}}$ be a sequence of parameter vectors such that $\tilde{l}_{\mathbf{n}_k}(\gamma_k) - \tilde{l}_{\mathbf{n}_k}(\theta)$ converges to zero as k goes to infinity. Then γ_k converges to θ .*

We now have the required tools to establish consistency.

Lemma 9 (Uniform convergence in probability of the likelihood function). *The likelihood function $l_{\mathbf{n}_k}(\cdot)$ converges uniformly in probability to $\tilde{l}_{\mathbf{n}_k}(\cdot)$ over the parameter set Θ as k goes to infinity.*

With these lemmata we have all the necessary results to establish Theorem 1. This theorem is important as it establishes the efficiency of our estimator. We contrast our results with those of Dahlhaus and Künsch (1987), Guyon (1982), as well as Fuentes (2007). The insight from Theorem 1, as compared to the insight of the need for tapering provided by Dahlhaus and Künsch (1987) is clear. The aim of this paper is to balance computational tractability with estimation performance. Very standard assumptions allow us to still derive the results required for estimation.

4.4 Asymptotic distribution

We now study the asymptotic distribution of our estimates within the increasing-domain asymptotics framework. In this section, for simplicity, we only consider the scenario of a fully observed grid, as we impose $g_{\mathbf{s}} = 1$ for all points \mathbf{s} of the grid. We first need to understand better the behaviour of quantities of the form $|\mathbf{n}|^{-1} \sum_{\omega \in \Omega_{\mathbf{n}_k}} w_k(\omega) I_{\mathbf{n}}(\omega)$, for

some weights w_k . In Proposition 1, we showed that under mild conditions, their variance was vanishing, with a rate inversely proportional the number of observed points. In Proposition 2, by writing this quantity as a Toeplitz quadratic form in the random vector \mathbf{X} , and by extending a result by Grenander and Szegö (1958), we show that this quantity is asymptotically normally distributed, under mild conditions on the family of functions $w_k(\cdot)$. Before getting there, we need the following intermediary result.

Lemma 10 (Upper bound on the spectral norm of the covariance matrix). *The spectral norm of $C_{\mathbf{X}}$ is bounded according to*

$$\|C_{\mathbf{X}}\| \leq f_{\delta, \max}, \quad \|C_{\mathbf{X}}^{-1}\| \leq f_{\delta, \min}^{-1}.$$

Proof. Please see the Appendix. □

Proposition 2 (Asymptotic normal distribution of bounded linear combinations of the periodogram). *Let $X(\mathbf{s})$, $\mathbf{s} \in \mathbb{R}^d$ be a homogeneous Gaussian process observed on the lattice $\mathcal{J}_{\mathbf{n}}$. Let $w_k(\cdot)$, $k \in \mathbb{N}$ be a family of real-valued functions defined on \mathcal{T}^d bounded above and below by two constants, denoted $M_W, m_W > 0$ respectively. Additionally, assume $g_{\mathbf{s}} = 1, \forall \mathbf{s} \in \mathcal{J}_{\mathbf{n}_k}$. Then $|\mathbf{n}|^{-1} \sum_{\omega \in \Omega_{\mathbf{n}_k}} w_k(\omega) I_{\mathbf{n}}(\omega)$ is asymptotically normally distributed.*

Proof. Please see the Appendix. □

We now have the required tools to conclude to the asymptotic normality of our estimates, which is the result of the next theorem. This theorem will require one additional assumption, which we now define.

Assumption 2 (Convergence rate assumptions).

1. *The interior of Θ is non-null and the true length- p parameter vector $\boldsymbol{\theta}$ lies in the interior of Θ .*
2. *The quantity $\bar{I}_{\mathbf{n}_k}(\boldsymbol{\omega}; \boldsymbol{\theta})$ admits second derivatives with respect to the parameter vector, and those second derivatives are continuous and upper-bounded in absolute value, independently of $\boldsymbol{\omega}$ and $\boldsymbol{\theta}$, by a constant denoted $M_{\partial^2} > 0$.*
3. *The spectral norm of*

$$\left(|\mathbf{n}_k|^{-1} \sum_{\omega \in \Omega} \bar{I}_{\mathbf{n}_k}(\boldsymbol{\omega}; \boldsymbol{\theta})^{-2} \nabla_{\boldsymbol{\theta}} \bar{I}_{\mathbf{n}_k}(\boldsymbol{\omega}; \boldsymbol{\theta}) \nabla_{\boldsymbol{\theta}} \bar{I}_{\mathbf{n}_k}(\boldsymbol{\omega}; \boldsymbol{\theta})^T \right)^{-1} \quad (24)$$

is upper-bounded independently of k .

Theorem 2 (Asymptotic normality of estimates). *Under the sets of Assumptions 1 and 2, if $g_{\mathbf{s}} = 1, \forall \mathbf{s} \in \mathcal{J}_{\mathbf{n}}$, the estimate $\hat{\boldsymbol{\theta}}$ is asymptotically normally distributed, and converges at rate $|\mathbf{n}_k|^{-1/2}$.*

Proof. Please see the Appendix. □

This shows the ability of our proposed estimation method to combine computational and statistical efficiency, for a wide variety of scenarios.

4.5 Estimating standard errors

We now seek to derive how to estimate the standard error of $\widehat{\boldsymbol{\theta}}$, as Theorem 2 only determines the rate. Using equations (60) and (63) from the Appendix, we obtain an approximation of its variance provided in the following proposition.

Proposition 3 (Exact form of the variance). *The covariance matrix of the quasi-likelihood estimator takes the form of*

$$\text{var} \left\{ \widehat{\boldsymbol{\theta}} \right\} \approx \boldsymbol{\mathcal{H}}^{-1}(\boldsymbol{\theta}) \text{var} \left\{ \nabla \ell_M(\boldsymbol{\theta}) \right\} \boldsymbol{\mathcal{H}}^{-1}(\boldsymbol{\theta}), \quad (25)$$

with the covariance matrix of the score taking the form of

$$\text{cov} \left\{ \frac{\partial \ell_M(\boldsymbol{\theta})}{\partial \theta_p}, \frac{\partial \ell_M(\boldsymbol{\theta})}{\partial \theta_q} \right\} = |\mathbf{n}|^{-2} \sum_{\boldsymbol{\omega}_1 \in \Omega_{\mathbf{n}}} \sum_{\boldsymbol{\omega}_2 \in \Omega_{\mathbf{n}}} \frac{\partial \bar{I}_{\mathbf{n}}(\boldsymbol{\omega}_1; \boldsymbol{\theta})}{\partial \theta_p} \frac{\partial \bar{I}_{\mathbf{n}}(\boldsymbol{\omega}_2; \boldsymbol{\theta})}{\partial \theta_q} \frac{\text{cov} \{ I_{\mathbf{n}}(\boldsymbol{\omega}_1), I_{\mathbf{n}}(\boldsymbol{\omega}_2) \}}{\bar{I}_{\mathbf{n}}^2(\boldsymbol{\omega}_1; \boldsymbol{\theta}) \bar{I}_{\mathbf{n}}^2(\boldsymbol{\omega}_2; \boldsymbol{\theta})}. \quad (26)$$

The computation that appears in (26) does not scale well for large grid sizes, as it scales like $|\mathbf{n}|^2$. We instead propose a Monte Carlo implementation to speed this up. The dominant terms in (26) correspond to $\boldsymbol{\omega}_1 = \boldsymbol{\omega}_2$. We approximate the sum over the rest of the terms, i.e., our approximation takes the form:

$$\begin{aligned} \text{cov} \left\{ \frac{\partial \ell_M(\boldsymbol{\theta})}{\partial \theta_p}, \frac{\partial \ell_M(\boldsymbol{\theta})}{\partial \theta_q} \right\} &= \frac{1}{|\mathbf{n}|^2} \sum_{\boldsymbol{\omega}_1 \in \Omega_{\mathbf{n}}} \left\{ \frac{\partial \bar{I}_{\mathbf{n}}(\boldsymbol{\omega}_1; \boldsymbol{\theta})}{\partial \theta_p} \frac{\partial \bar{I}_{\mathbf{n}}(\boldsymbol{\omega}_1; \boldsymbol{\theta})}{\partial \theta_q} \frac{\text{var} \{ I_{\mathbf{n}}(\boldsymbol{\omega}_1) \}}{\bar{I}_{\mathbf{n}}^4(\boldsymbol{\omega}_1; \boldsymbol{\theta})} \right\} \\ &+ \frac{n^2 - 2n + 1}{M|\mathbf{n}|^2} \sum_{i=1 \dots M} \frac{\partial \bar{I}_{\mathbf{n}}(\boldsymbol{\omega}_{1,i}; \boldsymbol{\theta})}{\partial \theta_p} \frac{\partial \bar{I}_{\mathbf{n}}(\boldsymbol{\omega}_{2,i}; \boldsymbol{\theta})}{\partial \theta_q} \frac{\text{cov} \{ I_{\mathbf{n}}(\boldsymbol{\omega}_{1,i}), I_{\mathbf{n}}(\boldsymbol{\omega}_{2,i}) \}}{\bar{I}_{\mathbf{n}}^2(\boldsymbol{\omega}_{1,i}; \boldsymbol{\theta}) \bar{I}_{\mathbf{n}}^2(\boldsymbol{\omega}_{2,i}; \boldsymbol{\theta})}, \end{aligned}$$

where the $\boldsymbol{\omega}_{1,i}, \boldsymbol{\omega}_{2,i}, i = 1 \dots M$ are uniformly and independently sampled from the set of Fourier frequencies under the requirement $\boldsymbol{\omega}_{1,i} \neq \boldsymbol{\omega}_{2,i}$. Note that if tapering is used, one should consider a few coefficients near the main diagonal in the above approximation, as tapering generates strong short-range correlation in the frequency domain.

The covariances of the periodogram at two distinct Fourier frequencies can be approximated by Riemann approximation of the two integrals that appear in the expression below, before taking squared absolute values and summing,

$$\begin{aligned} \text{cov} \{ I_{\mathbf{n}}(\boldsymbol{\omega}_{1,i}), I_{\mathbf{n}}(\boldsymbol{\omega}_{2,i}) \} &= |\mathbf{n}|^{-1} \left(\left| \int_{-\pi}^{\pi} \tilde{f}(\lambda) \mathcal{D}_{\mathbf{n}}(\lambda - \boldsymbol{\omega}_{1,i}) \mathcal{D}_{\mathbf{n}}^*(\lambda - \boldsymbol{\omega}_{2,i}) d\lambda \right|^2 \right. \\ &\quad \left. + \left| \int_{-\pi}^{\pi} \tilde{f}(\lambda) \mathcal{D}_{\mathbf{n}}(\lambda - \boldsymbol{\omega}_{1,i}) \mathcal{D}_{\mathbf{n}}^*(\lambda + \boldsymbol{\omega}_{2,i}) d\lambda \right|^2 \right). \end{aligned}$$

In the above, \tilde{f} is the following approximation to the spectral density, which can be computed by a DFT,

$$\tilde{f}(\lambda) = \sum_{\mathbf{u} \in \prod_{i=1}^d [-(n_i-1) \dots (n_i-1)]} c_X(\mathbf{u}; \boldsymbol{\theta}) \exp(-i\lambda \cdot \mathbf{u}),$$

and $\mathcal{D}_{\mathbf{n}}(\lambda)$ is the non-centred *modified* (due to the modulation $g_{\mathbf{s}}$) Dirichlet kernel of order \mathbf{n} given by

$$\mathcal{D}_{\mathbf{n}}(\lambda) = \sum_{\mathbf{s} \in \mathcal{J}_{\mathbf{n}}} g_{\mathbf{s}} \exp(i\lambda \cdot \mathbf{s}),$$

where for clarity we omit the dependence on the modulation $g_{\mathbf{s}}$ in the notation. Finally we compute the derivatives of $\bar{I}_{\mathbf{n}}(\boldsymbol{\omega}; \boldsymbol{\theta})$ as follows,

$$\nabla_{\boldsymbol{\theta}} \bar{I}_{\mathbf{n}}(\boldsymbol{\omega}; \boldsymbol{\theta}) = \sum_{\mathbf{u} \in \mathbb{Z}^d} \nabla_{\boldsymbol{\theta}} \bar{c}_X(\mathbf{u}; \boldsymbol{\theta}) \exp(-i\boldsymbol{\omega} \cdot \mathbf{u}). \quad (27)$$

5 Simulation Studies and Data Analysis

In this section we present simulation studies and a real data analysis that demonstrate the performance of our debiased Whittle method. The simulations presented in Section 5.1 address the estimation of the range parameter of a Matérn process, whose slope parameter is known, observed over a full rectangular grid. These simulations corroborate our theoretical results on the optimal convergence rate of our estimator despite edge effects, in contrast to the standard Whittle method. Our second simulation study in Section 5.2 shows how our estimation procedure extends the computational benefits of frequency-domain methods to non-rectangular shapes of data, where we compare parameter estimates with those of Guinness and Fuentes (2017). Finally, in Section 5.3 we demonstrate the performance of debiased Whittle when applied to topographical datasets obtained from Venus.

5.1 Estimation from a fully-observed rectangular grid of data

We simulate from the isotropic Matérn model family, which corresponds to the following covariance function,

$$c_X(\mathbf{u}) = \sigma^2 \frac{2^{1-\nu}}{\Gamma(\nu)} \left(\sqrt{2\nu} \frac{\|\mathbf{u}\|}{\rho} \right)^{\nu} \cdot K_{\nu} \left(\sqrt{2\nu} \frac{\|\mathbf{u}\|}{\rho} \right), \quad (28)$$

where $K_{\nu}(x)$ is a Bessel-function. We consider the problem of estimating the range parameter ρ , which is fixed to 10 units, while the amplitude $\sigma^2 = 1$ and the slope parameter $\nu \in \{\frac{1}{2}, \frac{3}{2}\}$ are fixed and known. Inference is achieved from simulated data on two-dimensional rectangular grids of increasing sizes, specifically $\{2^s : s = 4, \dots, 8\}$ in each dimension.

We implement four inference methods:

- (1) The debiased Whittle method, i.e., the estimate derived from (7);
- (2) The debiased Whittle method combined with a taper, specifically the estimate derived from (7) with $g_{\mathbf{s}}$ proportional to a Hanning taper;
- (3) The standard Whittle likelihood, i.e., estimators obtained by replacing $\bar{I}_{\mathbf{n}}(\boldsymbol{\omega}; \boldsymbol{\theta})$ with $f_X(\boldsymbol{\omega})$ in (5) and then minimizing (7);

- (4) The standard Whittle likelihood combined with tapering using a Hanning taper, again derived from (7) fitting to $f_X(\boldsymbol{\omega})$.

For each configuration of the slope parameter and grid size, we report summary statistics corresponding to 1,000 independently realized random fields. We report bias, standard deviation and root mean-squared error for $\nu = 0.5$ and $\nu = 1.5$ in Figures 2 and 3, respectively.

We first observe that the rate of the Whittle likelihood (3) is very poor, due to its large bias. It appears that tapering (4) leads to improved convergence rates when $\nu = 1.5$, although bias remains. On the contrary, the rates of our proposed method (1) and its tapered version (2) seem to not curb down even with larger grid sizes. This concurs with the theoretical results on the rate of convergence provided in Section 4. This example demonstrates that our debiased Whittle method balances the need for computational and statistical efficiency with large data sets.

In Figure 4 we report the empirical distribution of each estimator obtained from the 1,000 independent inference procedures for $\nu = \frac{1}{2}$. The four panels (a), (b), (c) and (d) show the distribution of estimates from the four methods stated on the previous page. The first two panels, (a) and (b), are broadly unbiased with estimates centred at $\rho = 10$ that converge quickly. The standard Whittle method (c) has issues with underestimation, tending towards $\rho = 5$. This bias is in large part due to aliasing not being accounted for combined with the relatively small value of $\nu = 0.5$; these effects are still present in the tapered estimates (d). As would be expected, in all four subplots the variance is decreasing with increasing sample size, at similar rates.

5.2 Estimation from a circular set of observations

In this section, we show how our debiased Whittle method extends to non-rectangular data. More specifically, we assume we only observe data within a circle with diameter 97 units. We consider the exponential covariance kernel given by

$$c_X(\mathbf{u}) = \sigma^2 \exp\left(-\frac{\|\mathbf{u}\|}{\rho}\right), \quad \mathbf{u} \in \mathbb{R}^2, \quad (29)$$

where $\sigma^2 = 1$ is fixed and known and we estimate the range parameter ρ whose true value is set to 5 units. A simulated sample is shown in Figure 5. We note that the case of a growing circle satisfies SCC, according to Lemma 3, and hence leads to consistency and asymptotic normality of our estimator.

A total number of 1,200 independent simulations are performed. For comparison, we compare to a recent method proposed by Guinness and Fuentes (2017), which is an approximation of the circulant embedding method developed by Stroud et al. (2017). Stroud et al. (2017) propose an Expectation Maximization iterative procedure, where the observed sample is embedded onto a larger grid that makes the covariance matrix *Block Circulant with Circulant Blocks* (BCCB), from where one can leverage the fast diagonalization procedure available for this class of matrices through the FFT algorithm. Guinness and Fuentes

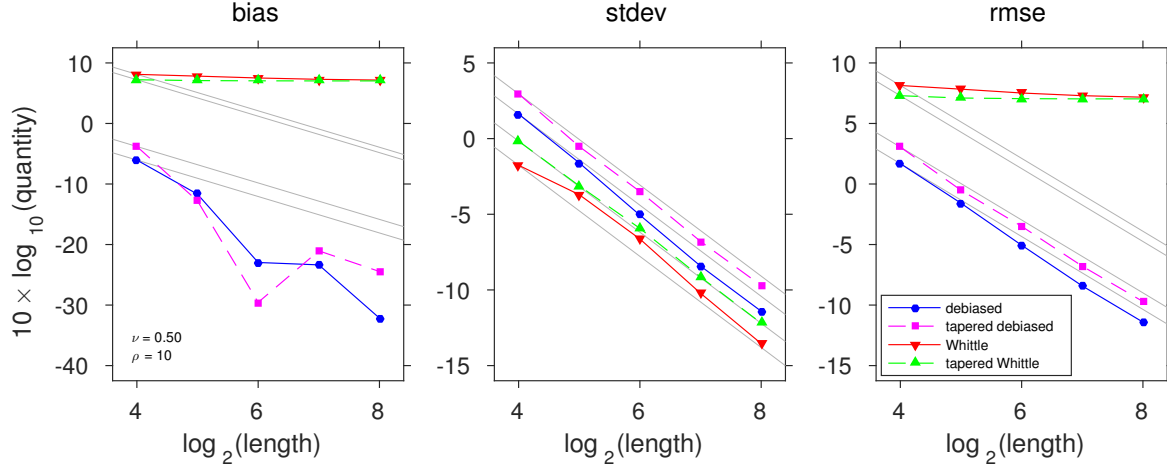


Figure 2: Bias, standard deviation, and root mean-squared error of estimates of the range parameter $\rho = 10$ of a Matérn process (28) with $\nu = \frac{1}{2}, \sigma^2 = 1$. The estimation method is identified by the line style, and gray lines functionally express the theoretical dependence on the square root of the sample size. The side length of the two-dimensional square grid is indicated by the x -axis, leading to a sample size of the length squared.

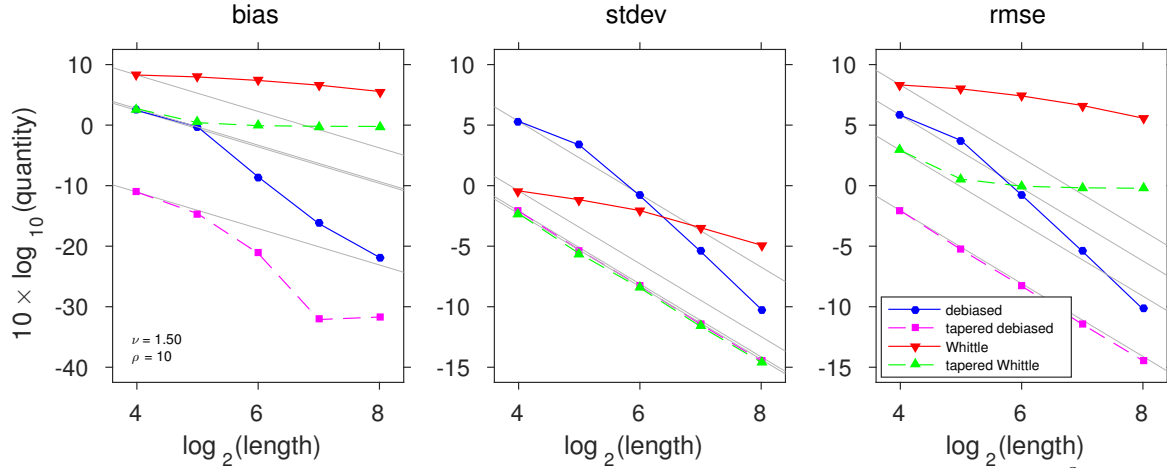


Figure 3: The same simulation setup as in Figure 2, but with $\nu = \frac{3}{2}$.

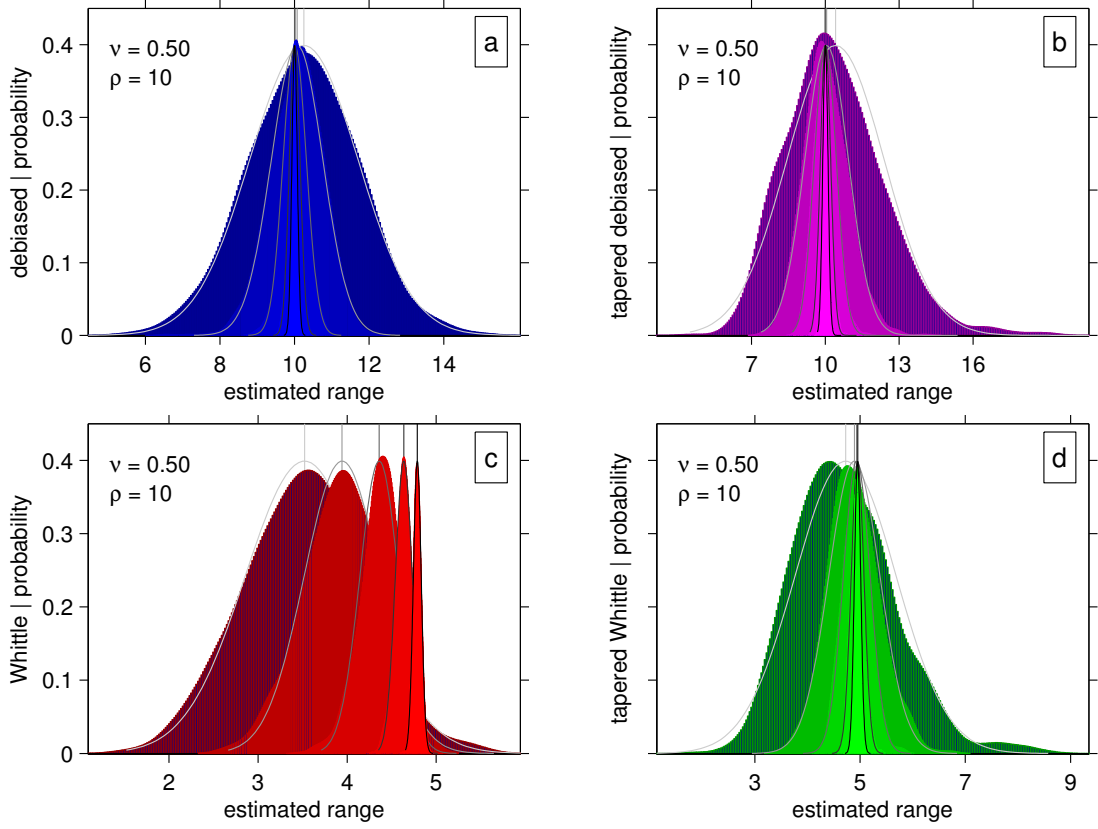


Figure 4: Nonparametric density estimates $\hat{\rho}$ of the estimated range parameter $\hat{\rho}$ ($\rho = 10$) for a Matérn random field (28), with $\sigma^2 = 1$ and $\nu = \frac{1}{2}$. The four subplots show different estimation methods of (a) debiased Whittle, (b) debiased Whittle with tapering, (c) standard Whittle, and (d) standard Whittle with tapering. The density estimate is shaded to reflect the size of the random field, with the darkest corresponding to total observations $|\mathbf{n}| = (2^4)^2$, and the shading incrementally taking a lighter colour for $|\mathbf{n}| = (2^5)^2, (2^6)^2, (2^7)^2, (2^8)^2$. Each density estimate is complemented by the best fitting Gaussian approximation as a solid black or fading gray line (black corresponds to $|\mathbf{n}| = (2^8)^2$ and the lightest gray to $|\mathbf{n}| = (2^4)^2$.)

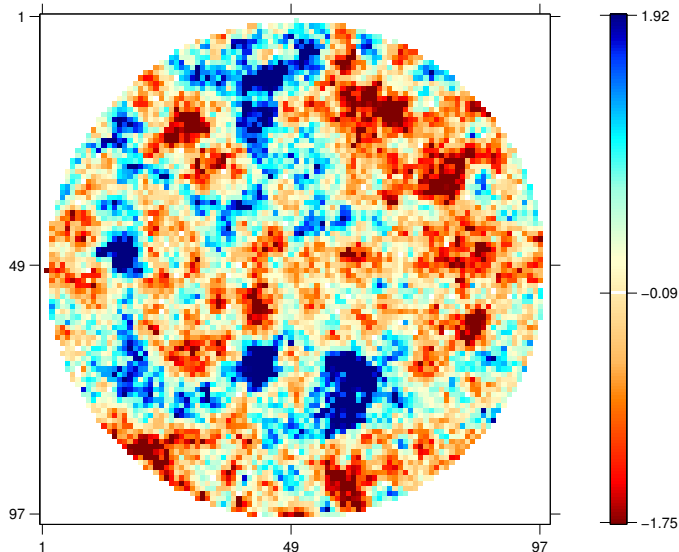


Figure 5: A random sample from an exponential covariance kernel (29) sampled on a regular grid with $\sigma^2 = 1$ and $\rho = 5$, that is only observed within a circle of diameter 97 units. The data outside the circle, shown in white, are not observed.

(2017) discuss that the size of the embedding grid is very large, making the imputations costly as well as the convergence of the iterative procedure slow. To address this they propose using a periodic approximation of the covariance function on an embedding grid which is much smaller than that required for the exact procedure. They show via simulations that using an embedding grid ratio of 1.25 along each axis leads to good approximations of the covariance function on the observed grid.

To implement the method developed by Guinness and Fuentes (2017), we use the code provided by the authors. We set a grid ratio of 1.25 to limit the computational cost, and implement the method with two choices of the number of imputations per iteration, $M = 1$ and $M = 20$. Each implementation is run for a number of 30 iterations for all samples.

Both our estimation method and that of Guinness and Fuentes (2017) are initialized with the estimates provided by the method proposed by Fuentes (2007). We show in Figure 6 (left panel) how debiased Whittle can achieve both computational and statistical efficiency. The 95 per cent confidence interval achieved by our estimate is similar to that obtained via the method of Guinness and Fuentes (2017) ($M=1$), however our method, despite also using an iterative maximization procedure, is significantly faster¹. As shown in Figure 6 (right panel), Guinness and Fuentes (2017) ($M=20$) leads to lower root mean-squared error but requires higher computational time.

¹Due to the fast computation and convergence of our maximization procedure we only report the final converged values of the debiased Whittle method in Figure 6.

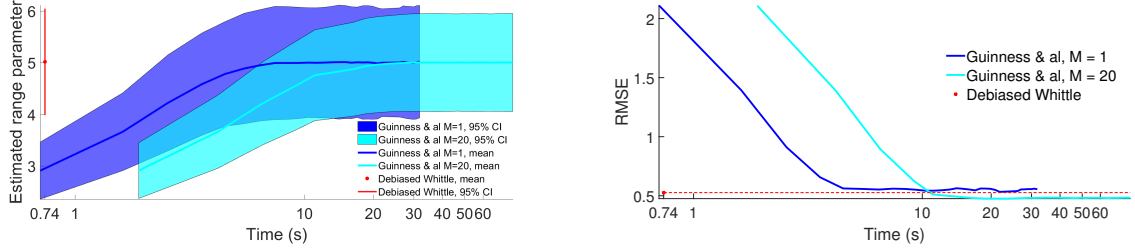


Figure 6: Mean and 95 per cent confidence intervals (left) and root mean-squared error (right) of estimates of the range parameter $\rho = 5$ of an exponential covariance model (29). Estimation is performed on a circular set of data with diameter 97 units, as shown in Figure 5. The converged estimates of the debiased Whittle method are compared to the iterated estimates of two implementations of Guinness and Fuentes (2017). The x -axis in both panels corresponds to the average computational time, as performed on an Intel(R) Core(TM) i7-7500U CPU 2.7–2.9 GHz processor.

5.3 Application to the study of Venus’ topography

In this section we apply our debiased Whittle method to the study of Venus’ topography. The motivation for modelling a planet’s topography using a parametric covariance model such as the Matérn process is multifaceted. For instance, we may expect that the combination of the slope and range parameters will carry important information about the geomorphological process or age of formation of the observed topography. This is because those parameters have some physical interpretation. The slope parameter can be related to the smoothness of the topography, and the range parameter tells about the typical distance over which two observed portions are uncorrelated.

Building on the work of Eggers (2013), we have selected four patches of data (including that shown in Figure 1 which corresponds to Patch 3), each sampled regularly on a complete rectangular grid. We compare three estimation procedures: the debiased Whittle method, the standard Whittle method, and the standard Whittle method with tapering (again using a Hanning taper). Parameter estimates are reported in Table 1. We also compare the value of the exact likelihood function taken at the estimated parameters for each estimation method in Table 2. Specifically, if $\hat{\theta}_M$ and $\hat{\theta}_W$ respectively denote the estimates obtained via the debiased Whittle and standard Whittle procedure, we compare $l_E(\hat{\theta}_M)$ and $l_E(\hat{\theta}_W)$, with $l_E(\cdot)$ denoting the exact likelihood function (which is expensive to evaluate but only needs to be done once for each analyzed method). The results in Table 2 show a much better fit of the model corresponding to the parameters estimated via the debiased Whittle method, in comparison to the parameters estimated via either standard Whittle or tapered Whittle. The estimates in Table 1 should be interpreted with care due to the challenges inherent in joint estimation of all three parameters of a Matérn covariance function (see, e.g., Zhang, 2004). However in all four patches we observe that the standard and tapered Whittle likelihood appear to overestimate the range while underestimating the smoothness, consistent with results found by Sykulski et al. (2019) for oceanographic time series.

Table 1: Estimates of the three parameters of a Matérn process (28) fitted to 4 patches of data of Venus’ topography. For each patch of data, three estimation methods are compared.

	Patch 1			Patch 2			Patch 3			Patch 4		
Parameter:	σ	ν	ρ	σ	ν	ρ	σ	ν	ρ	σ	ν	ρ
Debiased Whittle	1.2	0.5	17.7	1.2	0.7	6.8	2.1	0.5	36.5	1.5	0.6	15.0
Standard Whittle	1.6	0.3	62.7	1.8	0.3	73.9	1.5	0.2	77.3	1.7	0.3	87.3
Tapered Whittle	2.0	0.4	52.0	1.7	0.2	80.6	1.2	0.2	88.1	1.9	0.4	83.7

Table 2: Percentage of increase in the exact likelihood value at the estimated parameter values from Table 1 in comparison to the minimal value obtained among the three methods.

	Patch 1	Patch 2	Patch 3	Patch 4
Debiased Whittle	60.60	104.80	91.60	48.40
Standard Whittle	0	16.10	0	0
Tapered Whittle	23.20	0	53.90	25.20

To conclude our real-data analysis, we presented in Figure 1 a comparison of Patch 3 with three simulated samples, obtained using the Matérn model estimated using the debiased, standard and tapered Whittle methods respectively. This analysis supports the conclusion that the debiased Whittle method has found more appropriate parameter values for the model fit.

6 Discussion

Inferring the parameters of a spatial Gaussian process, imputing values of the process, or predicting out-of-range values, are all key problems in many different application areas of random fields. The key quantity that lets us perform such and other tasks is the likelihood function of the process observations, as most inferential tasks are normally formulated in terms of the likelihood via the Likelihood Principle). Unfortunately for most spatial problems computing the likelihood exactly is a computationally intractable problem.

The canonical solution to this challenge of big-data analysis is using Whittle’s approach to approximating the log-likelihood. This is based on (growing-domain) asymptotics and arguments that equate the Gaussian non-diagonal quadratic form with another Gaussian, nearly diagonal, form. For time series this argument is relatively straightforward; but is somewhat more complex for spatial data, where it is based on block-Toeplitz matrices (Tyrtyshnikov and Zamarashkin, 1998; Kazeev et al., 2013).

The approximation of the likelihood is an asymptotic result; and this is the root of any deteriorated performance of the Whittle likelihood-based parameter estimation of models of Gaussian processes in space. The bias of the periodogram, as an estimator of the

spectral density (which drives subsequent bias), decreases with rate $\mathcal{O}(|\mathbf{n}|^{-1/d})$ (Guyon, 1982; Dahlhaus and Künsch, 1987) in the case of a fully-observed rectangular lattice in d dimensions that grows at the same rate along all directions. A more precise result by Kent and Mardia (1996) shows that the approximation resulting from replacing the exact likelihood with the Whittle likelihood is driven by the size of the smallest side of the rectangular lattice. Dahlhaus (1983) proposed the use of tapering to remedy this issue. Despite the improved asymptotic behavior of the tapered periodogram, choosing an appropriate taper for a finite sample does require care. This is in particular true for non-rectangularly bounded data domains (Simons and Wang, 2011). Fuentes (2007) suggested to replace the missing points of a rectangular lattice with zeros as in (4) and correcting uniformly across frequencies for the amplitude of the periodogram, based on the ratio of the number of observed points to the total number of points in the grid. This only partly corrects for the bias of the periodogram that results from any non-trivial shape of the data.

Recently, Stroud et al. (2017) proposed a novel approach. Instead of approximating the multi-level Toeplitz covariance matrix of the rectangular lattice sample by a multi-level circulant matrix, one finds a larger lattice, termed an embedding, such that there exists a Block Circulant with Circulant Blocks (BCCB) matrix that is the covariance matrix of a Gaussian process on this extended lattice, and such that the covariance matrix of the real process is a submatrix of this extended matrix. One can then simulate efficiently the missing data on the extended lattice, and estimate the parameters of the models. This process can be iterated until a convergence criterion is met. This elegant method still suffers from computational issues, as the size of the embedding might be quite large. A solution suggested by Guinness and Fuentes (2017) is to use a circulant approximation of the covariance on a smaller rectangular lattice. The method is no longer exact, but Guinness and Fuentes (2017) showed via simulations that using small embeddings can in some cases provide a good compromise between statistical and computational efficiency.

In this paper we have revisited the root cause of why the approximation of the likelihood may deteriorate, while still requiring any proposed bias elimination to result in a computationally competitive method. This bias elimination is “built in” by fitting the periodogram to $\bar{I}_{\mathbf{n}}(\boldsymbol{\omega}; \boldsymbol{\theta})$, which is the expected periodogram. This is in contrast to estimating the bias and removing it, as this procedure would typically increase variance, and might lead to empirical spectral density estimates that are negative.

We have proposed a bias elimination method that is data-driven, automated and computationally practical for a number of realistic spatial sampling methods. What remains outstanding is the development of computationally competitive methods of a broad range of generically, non-uniformly sampled random fields. Our investigations also uncovered the theoretical class of models for which estimation is possible; those are strongly linked with growing-domain regularly sampled random fields. Studying this connection and its implications further, as well as deriving computationally efficient methods for inference of completely generically sampled fields, remain an outstanding research programme.

References

- Aharonson, O., Zuber, M. T., and Rothman, D. H. (2001), “Statistics of Mars’ topography from the Mars Orbiter Laser Altimeter: Slopes, correlations, and physical models,” *J. Geophys. Res.*, 106(E10), 23723–23735.
- Anitescu, M., Chen, J., and Stein, M. L. (2017), “An inversion-free estimating equations approach for Gaussian Process models,” *J. Comput. Graph. Stat.*, 26(1), 98–107.
- Bandyopadhyay, S., and Lahiri, S. N. (2009), “Asymptotic properties of discrete Fourier transforms for spatial data,” *Sankhya Ser. A.*, pp. 221–259.
- Bevilacqua, M., and Gaetan, C. (2015), “Comparing composite likelihood methods based on pairs for spatial Gaussian random fields,” *Stat. Comput.*, 25(5), 877–892.
- Candela, T., Renard, F., Klinger, Y., Mair, K., Schmittbuhl, J., and Brodsky, E. E. (2012), “Roughness of fault surfaces over nine decades of length scales,” *J. Geophys. Res.*, 117(B08409), 1–30.
- Cramér, H. (1946), *Mathematical Methods of Statistics*, Princeton, N.J.: Princeton Univ. Press.
- Dahlhaus, R. (1983), “Spectral analysis with tapered data,” *J. Time Ser. Anal.*, 4(3), 163–175.
- Dahlhaus, R., and Künsch, H. (1987), “Edge effects and efficient parameter estimation for stationary random fields,” *Biometrika*, 74(4), 877–882.
- Datta, A., Banerjee, S., Finley, A. O., and Gelfand, A. E. (2016), “Hierarchical nearest-neighbor Gaussian process models for large geostatistical datasets,” *J. Am. Stat. Assoc.*, 111(514), 800–812.
- Deb, S., Pourahmadi, M., and Wu, W. B. (2017), “An asymptotic theory for spectral analysis of random fields,” *Electron. J. Stat.*, 11(2), 4297–4322.
- Eggers, G. L. (2013), A regionalized maximum-likelihood estimation of the spatial structure of Venusian Topography, A. B. Thesis, Princeton University.
- Eom, K. B. (2001), “Long-correlation image models for textures with circular and elliptical correlation structures,” *IEEE T. Signal Process.*, 10(7), 1047–1055.
- Fernández-Casal, R., and Crujeiras, R. M. (2010), “Spatial dependence estimation using FFT of biased covariances,” *J. Stat. Plan. Inf.*, 140(9), 2653–2668.
- Fuentes, M. (2007), “Approximate likelihood for large irregularly spaced spatial data,” *J. Am. Stat. Assoc.*, 102(477), 321–331.

- Goff, J. A., and Arbic, B. K. (2010), “Global prediction of abyssal hill roughness statistics for use in ocean models from digital maps of paleo-spreading rate, paleo-ridge orientation, and sediment thickness,” *Ocean Modelling*, 32(1–2), 36–43.
- Grenander, U., and Szegö, G. (1958), *Toeplitz Forms and Their Applications*, Berkeley, Calif.: Univ. Calif. Press.
- Guillaumin, A. P., Sykulski, A. M., Olhede, S. C., Early, J. J., and Lilly, J. M. (2017), “Analysis of non-stationary modulated time series with applications to oceanographic surface flow measurements,” *J. Time Ser. Anal.*, 38(5), 668–710.
- Guinness, J. (2019), “Spectral density estimation for random fields via periodic embeddings,” *Biometrika*, 106, 267–286.
- Guinness, J., and Fuentes, M. (2017), “Circulant embedding of approximate covariances for inference from Gaussian data on large lattices,” *J. Comput. Graph. Stat.*, 26(1), 88–97.
- Guyon, X. (1982), “Parameter estimation for a stationary process on a d -dimensional lattice,” *Biometrika*, 69(1), 95–105.
- Heyde, C. C. (1997), *Quasi-Likelihood and its Application: A General Approach to Optimal Parameter Estimation*, New York: Springer.
- Horn, R. A., and Johnson, C. R. (1985), *Matrix analysis*, Cambridge, UK: Cambridge Univ. Press.
- Jain, S., Papadakis, M., Upadhyay, S., and Azencott, R. (2012), “Rigid motion invariant classification of 3-D textures,” *IEEE T. Image Proc.*, 21(5), 2449–2463.
- Jesus, J., and Chandler, R. E. (2017), “Inference with the Whittle likelihood: a tractable approach using estimating functions,” *J. Time Ser. Anal.*, 38(2), 204–224.
- Katzfuss, M. (2017), “A multi-resolution approximation for massive spatial datasets,” *J. Am. Stat. Assoc.*, 112(517), 201–214.
- Kaufman, C. G., Schervish, M. J., and Nychka, D. W. (2008), “Covariance tapering for likelihood-based estimation in large spatial data sets,” *J. Am. Stat. Assoc.*, 103(484), 1545–1555.
- Kazeev, V. A., Khoromskij, B. N., and Tyrtysnikov, E. E. (2013), “Multilevel Toeplitz matrices generated by tensor-structured vectors and convolution with logarithmic complexity,” *SIAM J. Sci. Comput.*, 35(3), A1511–A1536.
- Kent, J. T., and Mardia, K. V. (1996), “Spectral and circulant approximations to the likelihood for stationary Gaussian random fields,” *J. Stat. Plan. Inf.*, 50(3), 379–394.
- Koopmans, L. H. (1995), *The Spectral Analysis of Time Series*, 2 edn, San Diego, Calif.: Academic Press.

- Maggiori, E., Tarabalka, Y., Charpiat, G., and Alliez, P. (2017), “Convolutional neural networks for large-scale remote-sensing image classification,” *IEEE T. Geosci. Remote*, 55(2), 645–657.
- Mardia, K. V., and Marshall, R. J. (1984), “Maximum likelihood estimation of models for residual covariance in spatial regression,” *Biometrika*, 71(1), 135–146.
- Matsubara, T. (2004), “Correlation function in deep redshift space as a cosmological probe,” *Astroph. J.*, 615(2), 573–585.
- Matsuda, Y., and Yajima, Y. (2009), “Fourier analysis of irregularly spaced data on \mathbb{R}^d ,” *J. R. Stat. Soc., Ser. B*, 71(1), 191–217.
- North, G. R., Wang, J., and Genton, M. G. (2011), “Correlation models for temperature fields,” *J. Climate*, 24(22), 5850–5862.
- Rappaport, N. J., Konopliv, A. S., Kucinskas, A. B., and Ford, P. G. (1999), “An improved 360 degree and order model of Venus topography,” *Icarus*, 139, 19–31.
- Robinson, P. M., and Sanz, J. V. (2006), “Modified Whittle estimation of multilateral models on a lattice,” *J. Multivariate Anal.*, 97(5), 1090–1120.
- Sáez, M., Barceló, M. A., Tobias, A., Varga, D., Ocaña-Riola, R., Juan, P., and Mateu, J. (2012), “Space-time interpolation of daily air temperatures,” *J. Environ. Stat.*, 3(5).
- Scargle, J. D., Way, M. J., and Gazis, P. R. (2017), “Structure in the 3D galaxy distribution. III. Fourier transforming the Universe: Phase and power spectra,” *Astroph. J.*, p. 839:40.
- Shaby, B., and Ruppert, D. (2012), “Tapered covariance: Bayesian estimation and asymptotics,” *J. Comput. Graph. Stat.*, 21(2), 433–452.
- Simons, F. J., and Olhede, S. C. (2013), “Maximum-likelihood estimation of lithospheric flexural rigidity, initial-loading fraction and load correlation, under isotropy,” *Geophys. J. Int.*, 193(3), 1300–1342.
- Simons, F. J., and Wang, D. V. (2011), “Spatiospectral concentration in the Cartesian plane,” *Intern. J. Geomath.*, 2(1), 1–36.
- Stein, M. L. (2007), “Spatial variation of total column ozone on a global scale,” *Ann. Appl. Stat.*, 1(1), 191–210.
- Stroud, J. R., Stein, M. L., and Lysen, S. (2017), “Bayesian and maximum likelihood estimation for Gaussian processes on an incomplete lattice,” *J. Comput. Graph. Stat.*, 26(1), 108–120.
- Subba Rao, S. (2018), “Statistical inference for spatial statistics defined in the Fourier domain,” *Ann. Stat.*, 46(2), 469–499.

- Sun, Y., Bowman, K. P., Genton, M. G., and Tokay, A. (2015), “A Matérn model of the spatial covariance structure of point rain rates,” *Stoch. Env. Res. Risk A.*, 29(2), 411–416.
- Sykulski, A. M., Olhede, S. C., Guillaumin, A. P., Lilly, J. M., and Early, J. J. (2019), “The debiased Whittle likelihood,” *Biometrika*, 106(2), 251–266.
- Tyrtysnikov, E. E., and Zamarashkin, N. L. (1998), “Spectra of multilevel Toeplitz matrices: Advanced theory via simple matrix relationships,” *Lin. Alg. & Appl.*, 270(1-3), 15–27.
- Varin, C., Reid, N., and Firth, D. (2011), “An overview of composite likelihood methods,” *Stat. Sinica.*, 21, 5–42.
- Zhang, H. (2004), “Inconsistent estimation and asymptotically equal interpolations in model-based geostatistics,” *J. Am. Stat. Assoc.*, 99(465), 250–261.
- Zhang, H., and Zimmerman, D. L. (2005), “Towards reconciling two asymptotic frameworks in spatial statistics,” *Biometrika*, 92(4), 921–936.

Proofs of lemmata, propositions and theorems

Proof of Lemma 2

Proof. This comes as a consequence of the two following facts. First, two continuous functions on \mathcal{T}^d are equal if and only if their Fourier coefficients are equal. Second, for a sequence of full rectangular grids that grow unbounded in all directions, for any $\mathbf{u} \in \mathbb{Z}^d$ we have $c_{g,n_k}(\mathbf{u}) \rightarrow 1$ as k goes to infinity, see equation (14). \square

Proof of Lemma 3

Proof. The argument is very similar to that of Lemma 2, with the difference that for any $\mathbf{u} \in \mathbb{Z}^d$ we have that $c_{g,n_k}(\mathbf{u})$ converges to a positive constant (which might be strictly smaller than one) as k goes to infinity. \square

Proof of Theorem 1

Proof. We will show in Lemma 9 that $l_{\mathbf{n}_k}(\cdot)$ converges uniformly to $\tilde{l}_{\mathbf{n}_k}(\cdot)$ in probability, i.e., their difference converges uniformly to the zero function in probability. Hence the difference $l_{\mathbf{n}_k}(\hat{\boldsymbol{\theta}}_k) - \tilde{l}_{\mathbf{n}_k}(\hat{\boldsymbol{\theta}}_k)$ converges to zero in probability. Additionally, $l_{\mathbf{n}_k}(\hat{\boldsymbol{\theta}}_k) - \tilde{l}_{\mathbf{n}_k}(\boldsymbol{\theta})$ converges to zero in probability. Indeed, by definition, the parameter vector $\hat{\boldsymbol{\theta}}_k$ minimizes the function $l_{\mathbf{n}_k}(\cdot)$ over the parameter set Θ , and according to Lemma 4, the parameter vector $\boldsymbol{\theta}$ minimizes the function $\tilde{l}_{\mathbf{n}_k}(\cdot)$. We therefore have, by the triangle inequality,

$$\left| \tilde{l}_{\mathbf{n}_k}(\boldsymbol{\theta}) - \tilde{l}_{\mathbf{n}_k}(\hat{\boldsymbol{\theta}}_k) \right| \leq \left| l_{\mathbf{n}_k}(\hat{\boldsymbol{\theta}}_k) - \tilde{l}_{\mathbf{n}_k}(\hat{\boldsymbol{\theta}}_k) \right| + \left| l_{\mathbf{n}_k}(\hat{\boldsymbol{\theta}}_k) - \tilde{l}_{\mathbf{n}_k}(\boldsymbol{\theta}) \right|, \quad (30)$$

which converges to zero in probability. Making use of Lemma 8 we conclude that $\hat{\boldsymbol{\theta}}_k$ converges in probability to $\boldsymbol{\theta}$. \square

Proof of Proposition 1

Proof. Let $a_{\max} > 0$ be a finite constant such that $|a_{\mathbf{n}}(\boldsymbol{\omega})| \leq a_{\max}, \forall \boldsymbol{\omega} \in \mathcal{T}^2, \forall \mathbf{n} \in \mathbb{N}^2$. We start the proof assuming $g_{\mathbf{s}} = 1, \forall \mathbf{s} \in \mathcal{J}_{\mathbf{n}}$. We first make the observation that the sum of the periodogram values at the Fourier frequencies is the sample variance, since the Discrete Fourier Transform is orthonormal, so that

$$\begin{aligned} \text{var} \left\{ |\mathbf{n}|^{-1} \sum_{\boldsymbol{\omega} \in \Omega_{\mathbf{n}}} a_{\mathbf{n}}(\boldsymbol{\omega}) I_{\mathbf{n}}(\boldsymbol{\omega}) \right\} &\leq a_{\max}^2 \text{var} \left\{ |\mathbf{n}|^{-1} \sum_{\boldsymbol{\omega} \in \Omega_{\mathbf{n}}} I_{\mathbf{n}}(\boldsymbol{\omega}) \right\} \\ &= a_{\max}^2 |\mathbf{n}|^{-2} \text{var} \{ \mathbf{X}^T \mathbf{X} \}. \end{aligned}$$

Note that the first inequality is valid since the covariance of the periodogram at two Fourier frequencies $\boldsymbol{\omega}, \boldsymbol{\omega}'$ is positive for a Gaussian process, as a direct result of Isserlis' theorem. Indeed, letting $J(\boldsymbol{\omega}) = \frac{(2\pi)^{-d/2}}{\sqrt{\sum_{\mathbf{s} \in \mathcal{J}_{\mathbf{n}}} g_{\mathbf{s}}^2}} \sum_{\mathbf{s} \in \mathcal{J}_{\mathbf{n}}} g_{\mathbf{s}} X_{\mathbf{s}} \exp(-i\boldsymbol{\omega} \cdot \mathbf{s})$, we have,

$$\begin{aligned} \text{cov} \{I(\boldsymbol{\omega}), I(\boldsymbol{\omega}')\} &= \text{E} \{J(\boldsymbol{\omega}) J^*(\boldsymbol{\omega}) J(\boldsymbol{\omega}') J^*(\boldsymbol{\omega}')\} - \text{E} \{I(\boldsymbol{\omega}) I(\boldsymbol{\omega}')\} \\ &= \text{E} \{J(\boldsymbol{\omega}) J(\boldsymbol{\omega}')\} \text{E} \{J^*(\boldsymbol{\omega}) J^*(\boldsymbol{\omega}')\} + \text{E} \{J(\boldsymbol{\omega}) J^*(\boldsymbol{\omega}')\} \text{E} \{J^*(\boldsymbol{\omega}) J(\boldsymbol{\omega}')\} \\ &= |\text{E} \{J(\boldsymbol{\omega}) J(\boldsymbol{\omega}')\}|^2 + |\text{E} \{J^*(\boldsymbol{\omega}) J(\boldsymbol{\omega}')\}|^2. \end{aligned}$$

We study the term $\text{var} \{ \mathbf{X}^T \mathbf{X} \}$. We have, using Isserlis' theorem for Gaussian random variables,

$$\begin{aligned} \text{var} \{ \mathbf{X}^T \mathbf{X} \} &= \text{E} \left(\sum_{\mathbf{s} \in \mathcal{J}_{\mathbf{n}}} X_{\mathbf{s}}^2 \right)^2 - \left(\text{E} \sum_{\mathbf{s} \in \mathcal{J}_{\mathbf{n}}} X_{\mathbf{s}}^2 \right)^2 \\ &= \sum_{\mathbf{s} \in \mathcal{J}_{\mathbf{n}}} \sum_{\mathbf{s}' \in \mathcal{J}_{\mathbf{n}}} \text{E} \{X_{\mathbf{s}}^2 X_{\mathbf{s}'}^2\} - \text{E} \{X_{\mathbf{s}}^2\} \text{E} \{X_{\mathbf{s}'}^2\} \\ &= 2 \sum_{\mathbf{s} \in \mathcal{J}_{\mathbf{n}}} \sum_{\mathbf{s}' \in \mathcal{J}_{\mathbf{n}}} (\text{E} \{X_{\mathbf{s}} X_{\mathbf{s}'}\})^2 \end{aligned}$$

Now it is easy to see that this result generalizes to any modulation $g_{\mathbf{s}}$ meaning that we obtain,

$$\begin{aligned} \text{var} \left\{ |\mathbf{n}|^{-1} \sum_{\boldsymbol{\omega} \in \Omega_{\mathbf{n}}} a_{\mathbf{n}}(\boldsymbol{\omega}) I_{\mathbf{n}}(\boldsymbol{\omega}) \right\} &\leq 2c_{g, \mathbf{n}}(\mathbf{0})^{-2} a_{\max}^2 |\mathbf{n}|^{-2} \sum_{\mathbf{s} \in \mathcal{J}_{\mathbf{n}}} \sum_{\mathbf{s}' \in \mathcal{J}_{\mathbf{n}}} g_{\mathbf{s}} g_{\mathbf{s}'} (\text{E} \{X_{\mathbf{s}} X_{\mathbf{s}'}\})^2 \\ &\leq 2c_{g, \mathbf{n}}(\mathbf{0})^{-2} a_{\max}^2 |\mathbf{n}|^{-1} \sum_{\mathbf{u} \in \mathbb{Z}^d} c_{g, \mathbf{n}}(\mathbf{u}) c_X(\mathbf{u})^2 \\ &= 2a_{\max}^2 |\mathbf{n}|^{-1} c_{g, \mathbf{n}}(\mathbf{0})^{-1} \int_{\mathcal{T}^d} f_{X, \delta}(\boldsymbol{\omega})^2 d\boldsymbol{\omega}. \end{aligned}$$

\square

Proof of Lemma 4

Proof. The difference of the expected likelihood function at the true parameter vector and any parameter vector $\boldsymbol{\gamma} \in \Theta$ takes the form

$$\tilde{l}_{\mathbf{n}}(\boldsymbol{\gamma}) - \tilde{l}_{\mathbf{n}}(\boldsymbol{\theta}) = |\mathbf{n}|^{-1} \sum_{\boldsymbol{\omega} \in \Omega_{\mathbf{n}}} \phi \left(\frac{\bar{I}_{\mathbf{n}_k}(\boldsymbol{\omega}; \boldsymbol{\theta})}{\bar{I}_{\mathbf{n}_k}(\boldsymbol{\omega}; \boldsymbol{\gamma})} \right), \quad (31)$$

with $\phi : x \mapsto x - \log x - 1$. This function is non-negative and attains its minimum uniquely at $x = 1$. \square

Proof of Lemma 5

Proof. By combining equations (4) and (13) then the periodogram can be expressed as

$$I_{\mathbf{n}}(\boldsymbol{\omega}) = (2\pi)^{-d} |\mathbf{n}|^{-1} c_{g, \mathbf{n}}(\mathbf{0})^{-1} \left| \sum_{\mathbf{s} \in \mathcal{J}_{\mathbf{n}}} g_{\mathbf{s}} X_{\mathbf{s}} \exp(-i\boldsymbol{\omega} \cdot \mathbf{s}) \right|^2, \quad \boldsymbol{\omega} \in \mathcal{T}^d. \quad (32)$$

Making use of equation (9), we therefore have,

$$\bar{I}_{\mathbf{n}_k}(\boldsymbol{\omega}; \boldsymbol{\gamma}) = (2\pi)^{-d} c_{g, \mathbf{n}}(\mathbf{0})^{-1} \int_{\mathcal{T}^d} f_{\delta, X}(\boldsymbol{\omega} - \boldsymbol{\lambda}; \boldsymbol{\gamma}) \mathcal{F}_{\mathbf{n}_k}(\boldsymbol{\lambda}) d\boldsymbol{\lambda}. \quad (33)$$

Also,

$$\begin{aligned} \int_{\mathcal{T}^d} \mathcal{F}_{\mathbf{n}}(\boldsymbol{\omega}) d\boldsymbol{\omega} &= |\mathbf{n}|^{-1} \int_{\mathcal{T}^d} \left| \sum_{\mathbf{s} \in \mathcal{J}_{\mathbf{n}}} g_{\mathbf{s}} \exp(i\boldsymbol{\omega} \cdot \mathbf{s}) \right|^2 d\boldsymbol{\omega} \\ &= |\mathbf{n}|^{-1} \int_{\mathcal{T}^d} \sum_{\mathbf{s} \in \mathcal{J}_{\mathbf{n}}} \sum_{\mathbf{s}' \in \mathcal{J}_{\mathbf{n}}} g_{\mathbf{s}} g'_{\mathbf{s}'} \exp\{i\boldsymbol{\omega} \cdot (\mathbf{s}' - \mathbf{s})\} d\boldsymbol{\omega} \\ &= |\mathbf{n}|^{-1} \sum_{\mathbf{s} \in \mathcal{J}_{\mathbf{n}}} \sum_{\mathbf{s}' \in \mathcal{J}_{\mathbf{n}}} \int_{\mathcal{T}^d} g_{\mathbf{s}} g'_{\mathbf{s}'} \exp\{i\boldsymbol{\omega} \cdot (\mathbf{s}' - \mathbf{s})\} d\boldsymbol{\omega} \\ &= (2\pi)^d |\mathbf{n}|^{-1} \sum_{\mathbf{s} \in \mathcal{J}_{\mathbf{n}}} \sum_{\mathbf{s}' \in \mathcal{J}_{\mathbf{n}}} g_{\mathbf{s}} g'_{\mathbf{s}'} \delta_{\mathbf{s}, \mathbf{s}'} \\ &= (2\pi)^d c_{g, \mathbf{n}_k}(\mathbf{0}), \end{aligned}$$

which is a direct adaptation of a standard result for the Féjer kernel. Hence,

$$\begin{aligned} |\bar{I}_{\mathbf{n}_k}(\boldsymbol{\omega}; \boldsymbol{\gamma})| &\leq (2\pi)^{-d} c_{g, \mathbf{n}}(\mathbf{0})^{-1} \int_{\mathcal{T}^d} |f_{\delta, X}(\boldsymbol{\omega} - \boldsymbol{\lambda}; \boldsymbol{\gamma}) \mathcal{F}_{\mathbf{n}_k}(\boldsymbol{\lambda})| d\boldsymbol{\lambda} \\ &\leq (2\pi)^{-d} c_{g, \mathbf{n}}(\mathbf{0})^{-1} f_{\delta, \max} \int_{\mathcal{T}^d} |\mathcal{F}_{\mathbf{n}_k}(\boldsymbol{\lambda})| d\boldsymbol{\lambda} \\ &\leq f_{\delta, \max}. \end{aligned}$$

Similarly, we obtain the other inequality. \square

Proof of Lemma 6

Proof. We first observe, given equation (20), that

$$\tilde{l}_{\mathbf{n}_k}(\boldsymbol{\gamma}) - \tilde{l}_{\mathbf{n}_k}(\boldsymbol{\theta}) = |\mathbf{n}_k|^{-1} \sum_{\boldsymbol{\omega} \in \Omega_{\mathbf{n}_k}} \left\{ \frac{\bar{I}_{\mathbf{n}_k}(\boldsymbol{\omega}; \boldsymbol{\theta})}{\bar{I}_{\mathbf{n}_k}(\boldsymbol{\omega}; \boldsymbol{\gamma})} - \log \frac{\bar{I}_{\mathbf{n}_k}(\boldsymbol{\omega}; \boldsymbol{\theta})}{\bar{I}_{\mathbf{n}_k}(\boldsymbol{\omega}; \boldsymbol{\gamma})} - 1 \right\}. \quad (34)$$

As before, denoting $\phi : x \mapsto x - \log x - 1$, $x > 0$, and $g_{\mathbf{n}}(\boldsymbol{\omega})$ the piece-wise continuous function that maps any frequency of \mathcal{T}^d to the closest smaller Fourier frequency corresponding to the grid $\mathcal{J}_{\mathbf{n}}$, we have

$$\tilde{l}_{\mathbf{n}_k}(\boldsymbol{\gamma}) - \tilde{l}_{\mathbf{n}_k}(\boldsymbol{\theta}) = (2\pi)^{-d} \int_{\mathcal{T}^d} \phi \left(\frac{\bar{I}_{\mathbf{n}_k}(g(\boldsymbol{\omega}); \boldsymbol{\theta})}{\bar{I}_{\mathbf{n}_k}(g(\boldsymbol{\omega}); \boldsymbol{\gamma})} \right) d\boldsymbol{\omega}. \quad (35)$$

A Taylor expansion of $\phi(\cdot)$ around 1 gives, with $\psi(x) = (x - 1)^2$,

$$\phi(x) = \psi(x)(1 + \epsilon(x)), \quad (36)$$

where $\epsilon(x) \rightarrow 0$ as $x \rightarrow 1$. Therefore for any $\delta > 0$ there exists $\mu > 0$ such that for all x such that $|x - 1| \leq \mu$, $|\epsilon(x)| < \delta$. Now let, for all $k \in \mathbb{N}$,

$$\Pi_k = \left\{ \boldsymbol{\omega} \in T^d : \left| \frac{\bar{I}_{\mathbf{n}_k}(g(\boldsymbol{\omega}); \boldsymbol{\theta})}{\bar{I}_{\mathbf{n}_k}(g(\boldsymbol{\omega}); \boldsymbol{\gamma})} - 1 \right| \leq \mu \right\}. \quad (37)$$

We distinguish two cases:

1. If for some $\delta > 0$, the Lebesgue measure of Π_k does not converge to $(2\pi)^d$, equation (22) holds.
2. Otherwise, if for any $\delta > 0$ the Lebesgue measure of Π_k does converge to $(2\pi)^d$, we then have

$$\left| \tilde{l}_{\mathbf{n}_k}(\boldsymbol{\gamma}) - \tilde{l}_{\mathbf{n}_k}(\boldsymbol{\theta}) \right| = \int_{\Pi_k \cup \Pi_k^C} \psi \left(\frac{\bar{I}_{\mathbf{n}_k}(g(\boldsymbol{\omega}); \boldsymbol{\theta})}{\bar{I}_{\mathbf{n}_k}(g(\boldsymbol{\omega}); \boldsymbol{\gamma})} \right) \left\{ 1 + \epsilon \left(\frac{\bar{I}_{\mathbf{n}_k}(g(\boldsymbol{\omega}); \boldsymbol{\theta})}{\bar{I}_{\mathbf{n}_k}(g(\boldsymbol{\omega}); \boldsymbol{\gamma})} \right) \right\} d\boldsymbol{\omega}, \quad (38)$$

where Π_k^C denotes the complementary of Π_k as a subset of $[-\pi, \pi]^d$ and where the function $\epsilon(\cdot)$ was defined in equation (36). Denoting $h(\boldsymbol{\omega}; \boldsymbol{\theta}, \boldsymbol{\gamma}) = \frac{\bar{I}_{\mathbf{n}_k}(g(\boldsymbol{\omega}); \boldsymbol{\theta})}{\bar{I}_{\mathbf{n}_k}(g(\boldsymbol{\omega}); \boldsymbol{\gamma})}$ (note that this quantity also depends on k),

$$\begin{aligned} \tilde{l}_{\mathbf{n}_k}(\boldsymbol{\gamma}) - \tilde{l}_{\mathbf{n}_k}(\boldsymbol{\theta}) &= \int_{[-\pi, \pi]^d} \psi(h(\boldsymbol{\omega}; \boldsymbol{\theta}, \boldsymbol{\gamma})) d\boldsymbol{\omega} \\ &+ \int_{\Pi_k} \psi(h(\boldsymbol{\omega}; \boldsymbol{\theta}, \boldsymbol{\gamma})) \epsilon(h(\boldsymbol{\omega}; \boldsymbol{\theta}, \boldsymbol{\gamma})) d\boldsymbol{\omega} \\ &+ \int_{\Pi_k^C} \psi(h(\boldsymbol{\omega}; \boldsymbol{\theta}, \boldsymbol{\gamma})) \epsilon(h(\boldsymbol{\omega}; \boldsymbol{\theta}, \boldsymbol{\gamma})) d\boldsymbol{\omega}. \end{aligned}$$

We shall now show that the two last terms of the right-hand side of this equation are asymptotically vanishing, so that we can limit our study to the first term, which will turn out to take a simple form in relation to our definition of significant correlation contribution (SCC). Given the definition of Π_k we have,

$$\left| \int_{\Pi_k} \psi(h(\boldsymbol{\omega}; \boldsymbol{\theta}, \gamma)) \epsilon(h(\boldsymbol{\omega}; \boldsymbol{\theta}, \gamma)) d\boldsymbol{\omega} \right| \leq \delta \int_{\Pi_k} \psi(h(\boldsymbol{\omega}; \boldsymbol{\theta}, \gamma)) d\boldsymbol{\omega} \leq \delta \int_{T^d} \psi(h(\boldsymbol{\omega}; \boldsymbol{\theta}, \gamma)) d\boldsymbol{\omega},$$

where the two inequalities come from the fact that the function $\psi(\cdot)$ is non-negative. We also have

$$\left| \int_{\Pi_k^c} \psi(h(\boldsymbol{\omega}; \boldsymbol{\theta}, \gamma)) \epsilon(h(\boldsymbol{\omega}; \boldsymbol{\theta}, \gamma)) d\boldsymbol{\omega} \right| = o(1),$$

since the integrand is upper-bounded given Assumption 1.2 and since the measure of the set Π_k goes to zero. Hence we obtain, by the triangle inequality,

$$\left| \tilde{l}_{\mathbf{n}_k}(\gamma) - \tilde{l}_{\mathbf{n}_k}(\boldsymbol{\theta}) \right| \geq \left(\int_{T^d} \psi(h(\boldsymbol{\omega}; \boldsymbol{\theta}, \gamma)) d\boldsymbol{\omega} \right) (1 - \delta) + o(1).$$

We now study the term $(2\pi)^{-d} \int_{T^d} \psi(h(\boldsymbol{\omega}; \boldsymbol{\theta}, \gamma)) d\boldsymbol{\omega} = |\mathbf{n}_k|^{-1} \sum_{\boldsymbol{\omega} \in \Omega_{\mathbf{n}_k}} \left\{ \frac{\bar{I}_{\mathbf{n}_k}(\boldsymbol{\omega}; \boldsymbol{\theta})}{\bar{I}_{\mathbf{n}_k}(\boldsymbol{\omega}; \gamma)} - 1 \right\}^2$.

We observe that

$$\begin{aligned} |\mathbf{n}_k|^{-1} \sum_{\boldsymbol{\omega} \in \Omega_{\mathbf{n}_k}} \left\{ \bar{I}_{\mathbf{n}_k}(\boldsymbol{\omega}; \boldsymbol{\theta}) - \bar{I}_{\mathbf{n}_k}(\boldsymbol{\omega}; \gamma) \right\}^2 &= |\mathbf{n}_k|^{-1} \sum_{\boldsymbol{\omega} \in \Omega_{\mathbf{n}_k}} \bar{I}_{\mathbf{n}_k}(\boldsymbol{\omega}; \gamma)^2 \left\{ \frac{\bar{I}_{\mathbf{n}_k}(\boldsymbol{\omega}; \boldsymbol{\theta})}{\bar{I}_{\mathbf{n}_k}(\boldsymbol{\omega}; \gamma)} - 1 \right\}^2 \\ &\leq |\mathbf{n}_k|^{-1} f_{\max, \delta}^2 \sum_{\boldsymbol{\omega} \in \Omega_{\mathbf{n}_k}} \left\{ \frac{\bar{I}_{\mathbf{n}_k}(\boldsymbol{\omega}; \boldsymbol{\theta})}{\bar{I}_{\mathbf{n}_k}(\boldsymbol{\omega}; \gamma)} - 1 \right\}^2. \end{aligned}$$

Additionally, by Parseval's equality,

$$\begin{aligned} |\mathbf{n}_k|^{-1} \sum_{\boldsymbol{\omega} \in \Omega_{\mathbf{n}_k}} \left\{ \bar{I}_{\mathbf{n}_k}(\boldsymbol{\omega}; \boldsymbol{\theta}) - \bar{I}_{\mathbf{n}_k}(\boldsymbol{\omega}; \gamma) \right\}^2 &= \sum_{\mathbf{u} \in \mathbb{Z}^d} \left\{ \bar{c}_{\mathbf{n}_k}(\mathbf{u}; \boldsymbol{\theta}) - \bar{c}_{\mathbf{n}_k}(\mathbf{u}; \gamma) \right\}^2 \\ &= c_{g, \mathbf{n}_k}(\mathbf{0})^{-2} \sum_{\mathbf{u} \in \mathbb{Z}^d} c_{g, \mathbf{n}_k}(\mathbf{u})^2 \left\{ c_X(\mathbf{u}; \boldsymbol{\theta}) - c_X(\mathbf{u}; \gamma) \right\}^2 \\ &\geq \frac{1}{2} \underline{\lim}_{k \rightarrow \infty} S_k(\boldsymbol{\theta}, \gamma), \end{aligned}$$

where the last inequality holds for k sufficiently large, given the SCC assumption, see Definition 1. Therefore we obtain for k sufficiently large,

$$\left| \tilde{l}_{\mathbf{n}_k}(\gamma) - \tilde{l}_{\mathbf{n}_k}(\boldsymbol{\theta}) \right| \geq \frac{1}{2f_{\max, \delta}^2} (1 - \delta) \underline{\lim}_{k \rightarrow \infty} S_k(\boldsymbol{\theta}, \gamma) + o(1).$$

Choosing $\delta = 1/2$, we obtain equation (22). This concludes the proof. \square

Proof of Lemma 7

Proof. First we observe that for any fixed $\boldsymbol{\omega} \in \mathcal{T}^d$, $\bar{I}_{\mathbf{n}_k}(\boldsymbol{\omega}; \boldsymbol{\gamma}_k)$ converges to $\bar{I}_{\mathbf{n}_k}(\boldsymbol{\omega}; \boldsymbol{\gamma})$ as k goes to infinity. This comes from Assumption 1.2, where we have assumed an upper-bound on the derivative of the spectral density with respect to the parameter vector. In that case,

$$\begin{aligned} |\bar{I}_{\mathbf{n}_k}(\boldsymbol{\omega}; \boldsymbol{\gamma}_k) - \bar{I}_{\mathbf{n}_k}(\boldsymbol{\omega}; \boldsymbol{\gamma})| &\leq \left| \frac{(2\pi)^{-d}}{\sum_{s \in \mathcal{J}_n} g_s^2} \int_{\mathcal{T}^d} \{f_{X,\delta}(\boldsymbol{\omega} - \boldsymbol{\omega}'; \boldsymbol{\gamma}_k) - f_{X,\delta}(\boldsymbol{\omega} - \boldsymbol{\omega}'; \boldsymbol{\gamma})\} \mathcal{F}_n(\boldsymbol{\omega}') d\boldsymbol{\omega}' \right| \\ &\leq \frac{(2\pi)^{-d}}{\sum_{s \in \mathcal{J}_n} g_s^2} \int_{\mathcal{T}^d} |f_{X,\delta}(\boldsymbol{\omega} - \boldsymbol{\omega}'; \boldsymbol{\gamma}_k) - f_{X,\delta}(\boldsymbol{\omega} - \boldsymbol{\omega}'; \boldsymbol{\gamma})| \mathcal{F}_n(\boldsymbol{\omega}') d\boldsymbol{\omega}' \\ &\leq \frac{(2\pi)^{-d}}{\sum_{s \in \mathcal{J}_n} g_s^2} \int_{\mathcal{T}^d} M_{\partial_\theta} \|\boldsymbol{\gamma}_k - \boldsymbol{\gamma}\|_2 \mathcal{F}_n(\boldsymbol{\omega}') d\boldsymbol{\omega}' \\ &\leq M_{\partial_\theta} \|\boldsymbol{\gamma}_k - \boldsymbol{\gamma}\|_2 \frac{(2\pi)^{-d}}{\sum_{s \in \mathcal{J}_n} g_s^2} \int_{\mathcal{T}^d} \mathcal{F}_n(\boldsymbol{\omega}') d\boldsymbol{\omega}' \end{aligned}$$

which converges to zero as $\|\boldsymbol{\gamma}_k - \boldsymbol{\gamma}\|_2$ converges to zero by assumption.

Now using equation (20), we can again apply the Dominated Convergence Theorem to $(\tilde{l}_{\mathbf{n}_k}(\boldsymbol{\gamma}_k) - \tilde{l}_{\mathbf{n}_k}(\boldsymbol{\gamma}))_{k \in \mathbb{N}}$, using the bounds established in Lemma 5, and the $\boldsymbol{\omega}$ -pointwise convergence of $|\bar{I}_{\mathbf{n}_k}(\boldsymbol{\omega}; \boldsymbol{\gamma}_k) - \bar{I}_{\mathbf{n}_k}(\boldsymbol{\omega}; \boldsymbol{\gamma})|$ to zero. Hence $(\tilde{l}_{\mathbf{n}_k}(\boldsymbol{\gamma}_k) - \tilde{l}_{\mathbf{n}_k}(\boldsymbol{\gamma}))_{k \in \mathbb{N}}$ converges to zero, which concludes the proof. \square

Proof of Lemma 8

Proof. Assume, with the intent to reach a contradiction, that $(\boldsymbol{\gamma}_k)$ does not converge to $\boldsymbol{\theta}$. By compactness of Θ , there exists $\boldsymbol{\gamma} \in \Theta$ distinct from $\boldsymbol{\theta}$ and $(\boldsymbol{\gamma}_{j_k})$ a subsequence of $(\boldsymbol{\gamma}_k)$ such that $\boldsymbol{\gamma}_{j_k}$ converges to $\boldsymbol{\gamma}$. We then have, using the inverse triangle inequality,

$$|\tilde{l}_{\mathbf{n}_{j_k}}(\boldsymbol{\gamma}_{j_k}) - \tilde{l}_{\mathbf{n}_{j_k}}(\boldsymbol{\theta})| \geq \left| \tilde{l}_{\mathbf{n}_{j_k}}(\boldsymbol{\gamma}) - \tilde{l}_{\mathbf{n}_{j_k}}(\boldsymbol{\theta}) \right| - \left| \tilde{l}_{\mathbf{n}_{j_k}}(\boldsymbol{\gamma}_{j_k}) - \tilde{l}_{\mathbf{n}_{j_k}}(\boldsymbol{\gamma}) \right|. \quad (39)$$

The second term on the right-hand side of the above equation converges to zero according to Lemma 7 whereas the first term is asymptotically lower bounded according to Lemma 6. Therefore the quantity $|\tilde{l}_{\mathbf{n}_{j_k}}(\boldsymbol{\gamma}_{j_k}) - \tilde{l}_{\mathbf{n}_{j_k}}(\boldsymbol{\theta})|$ is asymptotically lower bounded, which contradicts the initial assumption that $\tilde{l}_{\mathbf{n}_k}(\boldsymbol{\gamma}_k) - \tilde{l}_{\mathbf{n}_k}(\boldsymbol{\theta})$ converges to zero. This concludes the proof, by obtaining a contradiction. \square

Proof of Lemma 9

Proof. We have

$$\begin{aligned} \tilde{l}_{\mathbf{n}_k}(\boldsymbol{\gamma}) - l_{\mathbf{n}_k}(\boldsymbol{\gamma}) &= |\mathbf{n}_k|^{-1} \sum_{\boldsymbol{\omega} \in \Omega_n} \left\{ \log \bar{I}_{\mathbf{n}_k}(\boldsymbol{\omega}; \boldsymbol{\gamma}) + \frac{\bar{I}_{\mathbf{n}_k}(\boldsymbol{\omega}; \boldsymbol{\theta})}{\bar{I}_{\mathbf{n}_k}(\boldsymbol{\omega}; \boldsymbol{\gamma})} - \log \bar{I}_{\mathbf{n}_k}(\boldsymbol{\omega}; \boldsymbol{\gamma}) - \frac{I_{\mathbf{n}_k}(\boldsymbol{\omega})}{\bar{I}_{\mathbf{n}_k}(\boldsymbol{\omega}; \boldsymbol{\gamma})} \right\} \\ &= |\mathbf{n}_k|^{-1} \sum_{\boldsymbol{\omega} \in \Omega_n} \frac{\bar{I}_{\mathbf{n}_k}(\boldsymbol{\omega}; \boldsymbol{\theta}) - I_{\mathbf{n}_k}(\boldsymbol{\omega})}{\bar{I}_{\mathbf{n}_k}(\boldsymbol{\omega}; \boldsymbol{\gamma})}. \end{aligned}$$

We note that

$$\mathbb{E} \left\{ \tilde{l}_{\mathbf{n}_k}(\gamma) - l_{\mathbf{n}_k}(\gamma) \right\} = 0. \quad (40)$$

Given that the quantity $\bar{l}_{\mathbf{n}_k}(\boldsymbol{\omega}; \gamma)^{-1}$ is deterministic and upper bounded independently of γ by $f_{\min, \delta}^{-1}$, we can use Proposition 1 to conclude that

$$\text{var} \left\{ \tilde{l}_{\mathbf{n}_k}(\gamma) - l_{\mathbf{n}_k}(\gamma) \right\} = \mathcal{O} \left\{ (c_{g, \mathbf{n}_k}(\mathbf{0}) |\mathbf{n}_k|)^{-1} \right\}, \quad (41)$$

where the big \mathcal{O} does not depend on γ . Thus using Chebychev's inequality

$$\tilde{l}_{\mathbf{n}_k}(\gamma) - l_{\mathbf{n}_k}(\gamma) = \mathcal{O}_P \left\{ (c_{g, \mathbf{n}_k}(\mathbf{0}) |\mathbf{n}_k|)^{-1/2} \right\}$$

This concludes the proof given Assumption 1.4. \square

Proof of Lemma 10

Proof. The proof is adapted from the one-dimensional case, see Guillaumin et al. (2017) and Sykulski et al. (2019). We first define the following isomorphism from $\{1, \dots, n_1\} \times \dots \times \{1, \dots, n_d\}$ to $\{1, \dots, |\mathbf{n}|\}$, that will be used for a change of variable:

$$j(j_1, \dots, j_d) = \sum_{k=1}^d \left\{ (j_k - 1) \prod_{j=1}^{k-1} n_j \right\}, \quad (42)$$

and $j_1(j), \dots, j_d(j)$ the component functions of its inverse. This isomorphism gives the index in the column vector \mathbf{X} of the observation at location (j_1, \dots, j_d) on the grid, given our choice of ordering.

Let $\boldsymbol{\alpha}$ be any complex-valued vector of \mathbb{C}^n , and denote $\boldsymbol{\alpha}^*$ its Hermitian transpose. We then have, using the above isomorphism for a change of variables,

$$\begin{aligned} \boldsymbol{\alpha}^* C_{\mathbf{X}} \boldsymbol{\alpha} &= \sum_{j, k=1}^{|\mathbf{n}|} \boldsymbol{\alpha}_j^* (C_{\mathbf{X}})_{j, k} \boldsymbol{\alpha}_k \\ &= \sum_{j_1=0}^{n_1-1} \cdots \sum_{j_d=1}^{n_d-1} \sum_{k_1=0}^{n_1-1} \cdots \sum_{k_d=1}^{n_d-1} \boldsymbol{\alpha}_{j(j_1, \dots, j_d)}^* (C_{\mathbf{X}})_{j(j_1, \dots, j_d), k(k_1, \dots, k_d)} \boldsymbol{\alpha}_{k(k_1, \dots, k_d)}. \end{aligned}$$

Here we use the fact that

$$(C_{\mathbf{X}})_{j(j_1, \dots, j_d), k(k_1, \dots, k_d)} = c_{\mathbf{X}}(k_1 - j_1, \dots, k_d - j_d),$$

so that

$$\begin{aligned}
\boldsymbol{\alpha}^* C_{\mathbf{X}} \boldsymbol{\alpha} &= \sum_{j_1=0}^{n_1-1} \cdots \sum_{j_d=1}^{n_d-1} \sum_{k_1=0}^{n_1-1} \cdots \sum_{k_d=1}^{n_d-1} \boldsymbol{\alpha}_{j(j_1, \dots, j_d)}^* \boldsymbol{\alpha}_{k(k_1, \dots, k_d)} \int_{\mathcal{T}^d} f_{X, \delta}(\boldsymbol{\omega}) e^{i((k_1-j_1)\omega_1 + \dots + (k_d-j_d)\omega_d)} d\boldsymbol{\omega} \\
&= \int_{\mathcal{T}^d} f_{X, \delta}(\boldsymbol{\omega}) \sum_{j_1=0}^{n_1-1} \cdots \sum_{j_d=1}^{n_d-1} \sum_{k_1=0}^{n_1-1} \cdots \sum_{k_d=1}^{n_d-1} \boldsymbol{\alpha}_{j(j_1, \dots, j_d)}^* \boldsymbol{\alpha}_{k(k_1, \dots, k_d)} e^{i((k_1-j_1)\omega_1 + \dots + (k_d-j_d)\omega_d)} d\boldsymbol{\omega} \\
&= \int_{\mathcal{T}^d} f_{X, \delta}(\boldsymbol{\omega}) \left| \sum_{j_1=0}^{n_1-1} \cdots \sum_{j_d=1}^{n_d-1} \boldsymbol{\alpha}_{j(j_1, \dots, j_d)} e^{i(j_1\omega_1 + \dots + j_d\omega_d)} \right|^2 d\boldsymbol{\omega} \\
&\leq f_{\delta, \max} \int_{\mathcal{T}^d} \left| \sum_{j_1=0}^{n_1-1} \cdots \sum_{j_d=1}^{n_d-1} \boldsymbol{\alpha}_{j(j_1, \dots, j_d)} e^{i(j_1\omega_1 + \dots + j_d\omega_d)} \right|^2 d\boldsymbol{\omega}.
\end{aligned}$$

By Parseval's equality, we obtain,

$$0 \leq \boldsymbol{\alpha}^* C_{\mathbf{X}} \boldsymbol{\alpha} \leq f_{\delta, \max} \|\boldsymbol{\alpha}\|_2^2, \quad (43)$$

where $\|\boldsymbol{\alpha}\|_2$ is the l_2 vector norm of the vector $\boldsymbol{\alpha}$. This concludes the proof of the upper bound. The lower bound can be derived in the same way, which concludes the proof. \square

Proof of Proposition 2

Proof. We only treat the scenario where $g_{\mathbf{s}} = 1, \forall \mathbf{s} \in \mathcal{J}_{n_k}$, i.e., we do not consider the situation of missing observations for this proposition. The proof is adapted from Grenander and Szegö (1958, p. 217). Denote

$$L_k = |\mathbf{n}_k|^{-1} \sum_{\boldsymbol{\omega} \in \Omega_{\mathbf{n}_k}} w_k(\boldsymbol{\omega}) I_{\mathbf{n}_k}(\boldsymbol{\omega}), \quad (44)$$

as a weighted sum of periodogram values, and $U_{\mathbf{n}_k}$ the multi-dimensional Fourier matrix corresponding to $\mathcal{J}_{\mathbf{n}}$. We have

$$L_k = |\mathbf{n}_k|^{-1} \mathbf{X}^* U_{\mathbf{n}_k}^* \text{diag}(w_k(\boldsymbol{\omega}_0), \dots, w_k(\boldsymbol{\omega}_{|\mathbf{n}_k|-1})) U_{\mathbf{n}_k} \mathbf{X}. \quad (45)$$

Denoting $W_k = |\mathbf{n}_k|^{-1} U_{\mathbf{n}_k}^* \text{diag}(w_k(\boldsymbol{\omega}_0), \dots, w_k(\boldsymbol{\omega}_{|\mathbf{n}_k|-1})) U_{\mathbf{n}_k}$, we then have

$$L_k = \mathbf{X}^* W_k \mathbf{X}, \quad (46)$$

which we regard as a quadratic form in the vector \mathbf{X} . Following Cramér (1946, p. 134), his formula 11.12.2, the characteristic function of the random variable L_k therefore takes the form of

$$\begin{aligned}
\phi_{L_k}(\alpha) &= \mathbb{E} \{ \exp(i\alpha L_k) \} \\
&= (2\pi)^{-n/2} |C_X(\boldsymbol{\theta})|^{-1/2} \int_{-\infty}^{\infty} \cdots \int_{-\infty}^{\infty} \exp \left\{ -x^* \left(-i\alpha W_k - \frac{1}{2} + C_X^{-1}(\boldsymbol{\theta}) \right) x \right\} dx_1 \cdots dx_n,
\end{aligned}$$

where for a square matrix A , $|A|$ denotes its determinant. Using a known result (Horn and Johnson, 1985) for complex-valued symmetric matrices, there exists a diagonal matrix D_k and a unitary matrix V_k such that

$$-i\alpha W_k + \frac{1}{2}C_X^{-1}(\boldsymbol{\theta}) = VD_kV^T. \quad (47)$$

By posing the change of variables $y = V^T x$ we obtain,

$$\phi_{L_k}(\alpha) = (2\pi)^{-n/2} |C_X(\boldsymbol{\theta})|^{-1/2} \prod_{j=1}^n \int_{-\infty}^{\infty} \exp\{-y^2 d_{j,k}\} dy, \quad (48)$$

where the $d_{j,k}, j = 1, \dots, n$ are the complex-valued elements of the diagonal matrix D_k from equation (47), and where we remind the reader that $|V| = 1$ since V is unitary. As we recognize integrals of the form $\int_{-\infty}^{\infty} \exp(-y^2) dy$ we obtain,

$$\begin{aligned} \phi_{L_k}(\alpha) &= 2^{-n/2} |C_X(\boldsymbol{\theta})|^{-1/2} \left| -i\alpha W_k + \frac{1}{2}C_X(\boldsymbol{\theta})^{-1} \right|^{-1/2} \\ &= \left| -2i\alpha C_X(\boldsymbol{\theta})W_k + I_{|\mathbf{n}|} \right|^{-1/2} \end{aligned}$$

Hence,

$$\log \phi_{L_k}(\alpha) = -\frac{1}{2} \log |I_{|\mathbf{n}_k|} - 2i\alpha C_X(\boldsymbol{\theta})W_k|.$$

Denoting with $\nu_{1,k}, \dots, \nu_{|\mathbf{n}_k|,k}$ the eigenvalues of $C_X(\boldsymbol{\theta})W_k$, we therefore have

$$\log \phi_{L_k}(\alpha) = -\frac{1}{2} \sum_{j=1}^{|\mathbf{n}_k|} \log(1 - 2i\alpha \nu_{j,k}). \quad (49)$$

According to Proposition 10 the spectral norm of C_X , the covariance matrix of \mathbf{X} , is upper-bounded by $f_{\max,\delta}$. The spectral norm of W_k is clearly upper-bounded by $|\mathbf{n}_k|^{-1}M_W$, since from the definition of W_k its eigenvalues are exactly

$$|\mathbf{n}_k|^{-1}w_k(\boldsymbol{\omega}_0), |\mathbf{n}_k|^{-1}w_k(\boldsymbol{\omega}_1), \dots, |\mathbf{n}_k|^{-1}w_k(\boldsymbol{\omega}_{|\mathbf{n}_k|-1}).$$

By property of the spectral norm of a product of matrices, we obtain,

$$|\mathbf{n}_k|^{-1}m_W f_{\min,\delta} \leq |\nu_{j,k}| \leq |\mathbf{n}_k|^{-1}M_W f_{\max,\delta}, \quad \forall j = 1, \dots, |\mathbf{n}_k|, k \in \mathbb{N}. \quad (50)$$

The variance of L_k is given by

$$\sigma_k^2 = \text{var}\{L_k\} = 2 \sum_{j=1}^{|\mathbf{n}_k|} \nu_{j,k}^2, \quad (51)$$

and therefore satisfies

$$2|\mathbf{n}_k|^{-1}(m_W f_{\min})^2 \leq \sigma_k^2 \leq 2|\mathbf{n}_k|^{-1}(M_W f_{\max,\delta})^2. \quad (52)$$

We also observe that

$$\frac{\nu_{j,k}}{\sigma_k} \rightarrow 0, \quad (k \rightarrow \infty), \quad (53)$$

uniformly, given the bounds determined in equations (50) and (52). Denote \underline{L}_k the standardized quantity $(L_k - \mathbb{E}\{L_k\})/\sigma_k$. After Taylor expansion of the logarithm terms to third order, its characteristic function takes the form of

$$\begin{aligned} \log \phi_{\underline{L}_k}(\alpha) &= -\frac{1}{2} \sum_{j=1}^{|\mathbf{n}_k|} \log \left(1 - \frac{2i\alpha\nu_{j,k}}{\sigma_k} \right) - i \frac{\alpha \sum_{j=1}^{|\mathbf{n}_k|} \nu_{j,k}}{\sigma_k} \\ &= -\frac{1}{2} \alpha^2 + \sum_{j=1}^{|\mathbf{n}_k|} \left[\frac{4}{3} \left(\frac{i\alpha\nu_{j,k}}{\sigma_k} \right)^3 + o \left\{ \left(\frac{i\alpha\nu_{j,k}}{\sigma_k} \right)^3 \right\} \right], \end{aligned} \quad (54)$$

where the small o is uniform and is denoted ϵ_k in what follows, to make it clear that it does not depend on j . The second term in equation (54) can be shown to become negligible as k goes to infinity, since

$$\left| \sum_{j=1}^{|\mathbf{n}_k|} \left[\frac{4}{3} \left(\frac{i\alpha\nu_{j,k}}{\sigma_k} \right)^3 + o \left\{ \left(\frac{i\alpha\nu_{j,k}}{\sigma_k} \right)^3 \right\} \right] \right| \leq \alpha^3 \sigma_k^{-3} \left(\frac{4}{3} + \epsilon_k \right) \sum_{j=1}^{|\mathbf{n}_k|} |\nu_{j,k}|^3 \quad (55)$$

$$\leq \alpha^3 \left(\frac{4}{3} + \epsilon_k \right) \frac{|\mathbf{n}_k|^{-2} M_W^3 f_{\max}^3}{|\mathbf{n}_k|^{-3/2} m_W^3 f_{\min}^3} \quad (56)$$

$$= \mathcal{O}(|\mathbf{n}_k|^{-1/2}). \quad (57)$$

We conclude that $\phi_{\underline{L}_k}(\alpha)$ converges to $\exp(-\frac{1}{2}\alpha^2)$, and therefore L_k is asymptotically standard normally distributed after appropriate normalization. \square

Proof of Theorem 2

Proof. The gradient of our quasi-likelihood function at the true parameter vector is given by

$$\nabla_{\theta} l_{\mathbf{n}_k}(\boldsymbol{\theta}) = |\mathbf{n}_k|^{-1} \sum_{\boldsymbol{\omega} \in \Omega_{\mathbf{n}_k}} \bar{I}_{\mathbf{n}_k}(\boldsymbol{\omega}; \boldsymbol{\theta})^{-2} \nabla_{\theta} \bar{I}_{\mathbf{n}_k}(\boldsymbol{\omega}; \boldsymbol{\theta}) (\bar{I}_{\mathbf{n}_k}(\boldsymbol{\omega}; \boldsymbol{\theta}) - I(\boldsymbol{\omega})). \quad (58)$$

According to Theorem 1, $\nabla_{\theta} l_{\mathbf{n}_k}(\boldsymbol{\theta})$ is asymptotically normally distributed, with mean the zero vector of \mathbb{R}^d . By expanding this gradient function at the true parameter value, we obtain

$$\nabla_{\theta} l_{\mathbf{n}_k}(\boldsymbol{\omega}; \boldsymbol{\theta}) = H(\boldsymbol{\theta}'_k)(\boldsymbol{\theta} - \hat{\boldsymbol{\theta}}_k), \quad (59)$$

where $H(\cdot)$ is the Hessian of $l_{\mathbf{n}_k}(\cdot)$ and $\boldsymbol{\theta}'_k$ is a parameter vector that converges in probability to the true parameter vector, since $\hat{\boldsymbol{\theta}}_k$ is consistent as per Theorem 1. Therefore,

$$\hat{\boldsymbol{\theta}}_k - \boldsymbol{\theta} = -H^{-1}(\boldsymbol{\theta}'_k) \nabla_{\theta} l_{\mathbf{n}_k}(\boldsymbol{\omega}; \boldsymbol{\theta}). \quad (60)$$

We now study the expected Hessian of the likelihood function taken at the true parameter vector, $\mathcal{H}(\boldsymbol{\theta})$. Direct calculations lead to

$$\mathcal{H}(\boldsymbol{\theta}) = |\mathbf{n}_k|^{-1} \sum_{\boldsymbol{\omega} \in \Omega_{\mathbf{n}_k}} \bar{I}_{\mathbf{n}_k}(\boldsymbol{\omega}; \boldsymbol{\theta})^{-2} \nabla_{\boldsymbol{\theta}} \bar{I}_{\mathbf{n}_k}(\boldsymbol{\omega}; \boldsymbol{\theta}) \nabla_{\boldsymbol{\theta}} \bar{I}_{\mathbf{n}_k}(\boldsymbol{\omega}; \boldsymbol{\theta})^T. \quad (61)$$

It can be shown, see Sykulski et al. (2019, p. 17 of their supplementary document) for instance, that in equation (60) the quantity $H(\boldsymbol{\theta}'_k)$ satisfies, if Assumption 2.2 holds,

$$H(\boldsymbol{\theta}'_k) = \mathcal{H}(\boldsymbol{\theta}) + \mathcal{O}_P(|\mathbf{n}_k|^{-1/2}) + o_P(1). \quad (62)$$

Hence we have, asymptotically,

$$H^{-1}(\boldsymbol{\theta}'_k) = \mathcal{H}^{-1}(\boldsymbol{\theta}) + o_P(1). \quad (63)$$

As the gradient at the true parameter vector $\nabla_{\boldsymbol{\theta}} l_{\mathbf{n}_k}(\boldsymbol{\omega}; \boldsymbol{\theta})$ is itself $\mathcal{O}_P(|\mathbf{n}_k|^{-1/2})$, and given Assumption 2.3 we obtain the stated result,

$$\hat{\boldsymbol{\theta}}_k - \boldsymbol{\theta} = \mathcal{O}_P(|\mathbf{n}_k|^{-1/2}). \quad (64)$$

□